
# NAVAL POSTGRADUATE SCHOOL

**MONTEREY, CALIFORNIA**

# THESIS

**CATHODE STALK COOLING SYSTEM FOR THE MK I QUARTERWAVE GUN**

by

Amanda B. Baxter

June 2012

Thesis Advisor: John Lewellen
Second Reader: Richard Swent

**Approved for public release; distribution is unlimited**

THIS PAGE INTENTIONALLY LEFT BLANK

| REPORT DOCUMENTATION PAGE | | | Form Approved OMB No. 0704-0188 |
|---|---|---|---|
| Public reporting burden for this collection of information is estimated to average 1 hour per response, including the time for reviewing instruction, searching existing data sources, gathering and maintaining the data needed, and completing and reviewing the collection of information. Send comments regarding this burden estimate or any other aspect of this collection of information, including suggestions for reducing this burden, to Washington headquarters Services, Directorate for Information Operations and Reports, 1215 Jefferson Davis Highway, Suite 1204, Arlington, VA 22202-4302, and to the Office of Management and Budget, Paperwork Reduction Project (0704-0188) Washington DC 20503. | | | |
| **1. AGENCY USE ONLY** ***(Leave blank)*** | **2. REPORT DATE** June 2012 | **3. REPORT TYPE AND DATES COVERED** Master's Thesis | |
| **4. TITLE AND SUBTITLE** Cathode Stalk Cooling System for the MK1 Quarterwave Gun | | **5. FUNDING NUMBERS** | |
| **6. AUTHOR(S)** Amanda B. Baxter | | | |
| **7. PERFORMING ORGANIZATION NAME(S) AND ADDRESS(ES)** Naval Postgraduate School Monterey, CA 93943-5000 | | **8. PERFORMING ORGANIZATION REPORT NUMBER** | |
| **9. SPONSORING /MONITORING AGENCY NAME(S) AND ADDRESS(ES)** N/A | | **10. SPONSORING/MONITORING AGENCY REPORT NUMBER** | |
| **11. SUPPLEMENTARY NOTES** The views expressed in this thesis are those of the author and do not reflect the official policy or position of the Department of Defense or the U.S. Government. IRB Protocol number _____N/A_____. | | | |
| **12a. DISTRIBUTION / AVAILABILITY STATEMENT** Approved for public release; distribution is unlimited | | **12b. DISTRIBUTION CODE** A | |

**13. ABSTRACT (maximum 200 words)**

The free electron laser (FEL) is of great interest to the United States Navy for shipboard use. The Naval Postgraduate School (NPS) Beam Physics Lab has designed and, in cooperation with other organizations, constructed a superconducting 500 MHz quarter-wave gun and photocathode drive laser system. The cathode of the gun is mounted onto a ~60 cm copper stalk assembly that will position and hold the cathode at the nose cone of the gun. This thesis will explore the necessity to cool the cathode stalk assembly that will have approximately 100 W of laser, RF, and radiated heat distributed on it. Based on the operational requirements of the MK I quarter-wave gun, a cooling system was designed to run liquid nitrogen internally through the stalk. Simulations were run on COMSOL to determine the effectiveness of the design, followed by the creation of a test stand to physically assess the cryogenic cooling system. Data was found verifying the applicability of the system. Recommendations are made for future experimentation using the cathode stalk cooling system test stand based on the results of this thesis.

| **14. SUBJECT TERMS TERMS** Free Electron Lasers, FEL, Cathode, Photocathode, Cryomodule, Cryogenic, Electron Gun, Superconducting, Quarter-wave Cavity | | | **15. NUMBER OF PAGES** 85 |
|---|---|---|---|
| | | | **16. PRICE CODE** |
| **17. SECURITY CLASSIFICATION OF REPORT** Unclassified | **18. SECURITY CLASSIFICATION OF THIS PAGE** Unclassified | **19. SECURITY CLASSIFICATION OF ABSTRACT** Unclassified | **20. LIMITATION OF ABSTRACT** UU |

NSN 7540-01-280-5500 Standard Form 298 (Rev. 2-89)
Prescribed by ANSI Std. 239-18

THIS PAGE INTENTIONALLY LEFT BLANK

**Approved for public release; distribution is unlimited**

# CATHODE STALK COOLING SYSTEM FOR THE MK 1 QUARTERWAVE GUN

Amanda B. Baxter
Lieutenant, United States Navy
B.S., Southern University and A&M College, 2006

Submitted in partial fulfillment of the
requirements for the degree of

**MASTER OF SCIENCE IN APPLIED PHYSICS**

from the

**NAVAL POSTGRADUATE SCHOOL**
**June 2012**

Author: Amanda B. Baxter

Approved by: John Lewellen
Thesis Advisor

Richard Swent
Second Reader

Andres Larraza
Chair, Department of Physics

THIS PAGE INTENTIONALLY LEFT BLANK

# ABSTRACT

The free electron laser (FEL) is of great interest to the United States Navy for shipboard use. The Naval Postgraduate School (NPS) Beam Physics Lab has designed and, in cooperation with other organizations, constructed a superconducting 500 MHz quarter-wave gun and photocathode drive laser system. The cathode of the gun is mounted onto a ~60 cm copper stalk assembly that will position and hold the cathode at the nose cone of the gun. This thesis will explore the necessity to cool the cathode stalk assembly that will have approximately 100 W of laser, RF, and radiated heat distributed on it. Based on the operational requirements of the MK I quarter-wave gun, a cooling system was designed to run liquid nitrogen internally through the stalk. Simulations were run on COMSOL to determine the effectiveness of the design, followed by the creation of a test stand to physically assess the cryogenic cooling system. Data was found verifying the applicability of the system. Recommendations are made for future experimentation using the cathode stalk cooling system test stand based on the results of this thesis.

THIS PAGE INTENTIONALLY LEFT BLANK

# TABLE OF CONTENTS


I. INTRODUCTION....1

II. FREE ELECTRON LASER DESCRIPTION....5
- A. INJECTOR....6
- B. LINEAR ACCELERATOR....7
- C. UNDULATOR....8
- D. OPTICAL CAVITY....8
- E. BEAM LINE SUPPORT COMPONENTS....9
- F. BEAM DUMP....9

III. FREE ELECTRON LASER THEORY....11
- A. THE PENDULUM EQUATION AND RESONANCE CONDITION....11
- B. OPTICAL WAVE EQUATION....15
- C. OPTICAL GAIN....17
- D. BEAM QUALITY....21

IV. DESIGN OF THE MK 1 SUPERCONDUCTING QUARTER-WAVE ELECTRON GUN....23
- A. GUN DESIGN....23
- B. INITIAL TESTING....28
- C. MOTIVATION FOR DEVELOPMENT OF A CATHODE STALK COOLING SYSTEM....28

V. CATHODE STALK TEST STAND AND COOLING SYSTEM DESIGN....31
- A. DETERMINING THE DESIGN....31
- B. TEST STAND FABRICATION....33

VI. CATHODE STALK TEST STAND EXPERIMENTAL RESULTS AND RECOMMENDATIONS FOR FURTHER TESTING....41
- A. INITIAL TESTS....42
- B. TESTING WITH LIQUID NITROGEN....45
  - 1. Initial Configuration....45
  - 2. $LN_2$ Fill System Modifications....47
- C. CONCLUSIONS....55

APPENDIX....59
- A. TEST STAND CATHODE STALK DIMENSIONS (CM)....59
- B. VACUUM HOUSING FOR TEST STAND (CM)....60
- C. INITIAL TEST STAND CONFIGURATION....61
- D. CHANGE TO TEST STAND CONFIGURATION....62
- E. FINAL CHANGE TO TEST STAND....63

LIST OF REFERENCES....65

INITIAL DISTRIBUTION LIST....67

THIS PAGE INTENTIONALLY LEFT BLANK

# LIST OF FIGURES


Figure 1. FEL Schematic (From [4]).....5
Figure 2. The accelerator is cooled with liquid helium to get the RF cavity to superconducting temperatures. A liquid nitrogen heat shield is used as a buffer from room temperatures to minimize the heat load on the helium (After [5]).....7
Figure 3. Schematic of linear undulator magnet orientation (From [6]).....8
Figure 4. Optical cavity for oscillator FEL (After [4])....9
Figure 5. Electron-Photon interaction. Here the red circles are the electrons interacting with the optical wavelength, the blue waves, and the undulator wavelength, the green wave (From [4]).....12
Figure 6. Electron Phase velocity at resonance (From [4]).....19
Figure 7. Electron phase velocity off-resonance (From [4]).....20
Figure 8. Strong optical fields (From [4]).....20
Figure 9. Cross section of the cavity with the coupler and cathode stalk installed (After [11]).....24
Figure 10. Detail of cathode stalk assembly with an inserted cathode (After [9]).....25
Figure 11. Top: Cathode stalk, without cathode, attached to mounting plate with Teflon spider in place Bottom: Detail of installed cathode on stalk tip (From [9])....26
Figure 12. Schematic of the RF control circuit (From [9]).....27
Figure 13. The top portion is a cut away of the cathode stalk with the cathode mounted on the tip. The maximum temperature is on the very tip of the stalk and is simulated to be 96.6 K. Dark blue is 77K.....32
Figure 14. Left: COMSOL simulation of flow through 1/8" copper tubing, resulting in a maximum flow rate of 6.1 ml/s. Figure 14. Right: Set up used for experimental testing of the helical design with water.....33
Figure 15. Top: Rhino model of test cathode stalk. Bottom: Completed test cathode stalk screwed into double sided flange used to mount into the test stand vacuum system. The stalk can be screwed apart at each place where it changes diameter as well as the tip.....34
Figure 16. Top Left: Rhino design of cooling coil in cut-away view of the cathode stalk. Top Right: Fabricated cooling coil used in test stand. Bottom Left: Vacuum system designed in Rhino utilizing models of crosses and nipples from Lesker.com. Bottom Right: Assembled vacuum chamber test stand.....34
Figure 17. Left: Design of double sided flange in Rhino. Right: Double sided flange being machined for use in the vacuum system. .....36
Figure 18. Test stand layout. .....36
Figure 19. Left: DT-670C-SD diode. Right: Cathode stalk with mounted diodes. The circles indicate the location of the diodes, with the one at the tip of the stalk being inside of the stalk.....37

Figure 20. The cathode stalk is wrapped with the heating cord and being tested, in conjunction with the diodes, with the variac prior to completing the assembly of the vacuum chamber. ....38
Figure 21. Left: Cut-away view of fill-pot (provided by Richard Swent). Right: The blue cylinder is the fill-pot. The dewar is connected to the top of the fill-pot, the cord connects the sensor to the liquid level controller. In this configuration the cooling coil exhausts to atmosphere. ....39
Figure 22. Cameras mounted to view tip of cathode stalk to record bending and deflection. ....40
Figure 23. Top: Illustration of temperature sensor diodes locations, T1 being inside of the cap at this position. Bottom: Spots where thermal camera was focused to obtain temperature. Note, HT3 is on the mounting flange connected directly to the cathode stalk. ....41
Figure 24. Plot of temperatures taken as applied power was increased, with error bars of 2 W. This data was taken prior to the LabVIEW program being established. ....43
Figure 25. Left: Demonstrates the pressure increases and drops over the duration of the applied power. Right: Plots the pressure change over time, better representing the pressure rise and decrease. ....44
Figure 26. The test stand is operating as expected, with temperatures T3 and T4 higher than the front of the stalk. T1 and T2 offer promising results in this initial phase. ....45
Figure 27. First attempt at cooling the cathode stalk beginning at room temperature with no heat applied. Pressure from opening the valve on the LN tank to fill the fill-pot had significant effects on the temperature, as did the amount of LN in the fill-pot. ....46
Figure 28. Test of cooling system without heat using a modified regulator valve. All temperatures readings are as expected with T4 being the highest due to its connection to the flange, and thus the outside world. ....48
Figure 29. Plot of cooling from room temperature to steady state, and then the gradual addition of power, stopping at 87 W. Temperature reached equilibrium at ~1844. ....49
Figure 30. The stalk was cooled with LN, once the temperatures were steady. At 1107 100 W of power was applied. The spike seen at 0815 was due to pressure from the LN tank into the fill-pot being too high. The tiny bumps that can be seen along T2 are caused by the filling of the fill-pot. ....50
Figure 31. The system operated optimally until the power was applied at 2052. Fluctuations occurred all the way up to when the variac was turned off at 2348. No fluctuations in temperature occurred after this time. ....51
Figure 32. Cooling worked nominally until power was added. The fill level on the fill-pot was increased to create a higher pressure and flow through the system, but fluctuations still occurred. ....52
Figure 33. At 1616 the variac was turned on to 64 percent of 120 V applying 100 W of power to the stalk. Once power was applied LN flow into the cooling

coil stopped. The malfunctions in the diode at T3 are apparent as dropouts in the temperature reading. ....53
Figure 34. Instead of the LN flow stopping it continued to cool the system, but with the fluctuations seen in previous tests.....54
Figure 35. At 1359 the variac was turned on at 20 percent (9 W) of 120 V, then at 1525 it was increased to 40 percent (37 W). The cooling system was able to manage the power applied at these times. At 1806 the variac was increased to 60 percent (87 W). Here the fluctuations immediately began. ...55

THIS PAGE INTENTIONALLY LEFT BLANK

# LIST OF ACRONYMS AND ABBREVIATIONS

| | |
|---|---|
| FEL | Free Electron Laser |
| HT | Housing Temperature |
| INP | Innovative Navy Prototype |
| LASER | Light Amplification by Simulated Emission of Radiation |
| LINAC | Linear Accelerator |
| LN | Liquid Nitrogen |
| MASER | Microwave Amplification by Stimulated Emission of Radiation |
| NC | Normal Conducting |
| NbTi | Niobium-Titanium |
| RF | Radiofrequency |
| SCA | Superconducting Accelerator |
| SRF | Superconducting Radiofrequency |
| SSA | Solid State Amplifier |
| T | Temperature |

THIS PAGE INTENTIONALLY LEFT BLANK

# ACKNOWLEDGMENTS

This research project would not have been possible without the support of many people. I wish to express my gratitude to my thesis advisor, Dr. John Lewellen, who was abundantly helpful and offered invaluable assistance, support and guidance. My deepest gratitude are also due to Dr. Richard Swent and Don Snyder without whose knowledge and assistance this experiment would not have been successful. The NPS Beam Physics Lab as a whole deserves my deepest appreciativeness for all of the help, instruction, and encouragement.

Special thanks to all of my friends and family who have supported me through every adventure. I owe this accomplishment to the love and understanding you have given me throughout the years and through the duration of my studies.

THIS PAGE INTENTIONALLY LEFT BLANK

# I. INTRODUCTION

This thesis focuses on creating a cooling system for the copper cathode stalk in the MK1 quarter-wave electron gun that may also be utilized in future derivations of the gun. While this thesis does not directly concentrate on the entirety of the free electron laser (FEL), it will be beneficial to understand a brief history of directed energy and the benefits of FELs over other types of lasers.

Almost a century ago, Albert Einstein laid the groundwork for the maser and laser when he established the theoretical foundations through a re-derivation of Planck's law of radiation. Concurrently, advances in electromagnetic theory led to the development of radar and components, such as magnetrons, microwave tubes, and klystrons, which allowed the production of coherent microwave radiation. Charles H. Townes demonstrated the maser in 1953, producing coherent electromagnetic waves. The maser was used as a foundation for developing the laser, which produces coherent optical waves. The term laser was coined by Gordon Gould a graduate student of Townes. In 1960, Theodore Maiman was the first to build and demonstrate a working laser. Maiman used a synthetic ruby crystal as his energy-absorbing material and a flash lamp as the excitation source. A photon beam was created using the flash lamp to pump energy into the ruby which allowed the excitation of electrons in the ground state to a higher state. When the electrons transitioned from the excited state back to a lower state they emitted a photon. These photons stimulated other excited atoms in the material to emit in phase with the incident photon, creating an outpouring of coherent photons, which were collected in a cavity that uses optical lenses and mirrors to direct and focus the photon beam. While Maiman's laser opened the door to the possibilities and uses of the laser, it also demonstrated that this type of laser would always suffer from physical limits related to the lasing medium (e.g. overheating, cracking, distorting). The gas lasers were the first high energy lasers, but were still limited in power production [1].

In 1973, the first chemical lasers were operational. These lasers were powerful and piqued military and industrial interests. The chemical lasers are limited as weapon systems by the amount of chemicals that must be carried in order to operate, the toxic and

corrosive nature of their feed and exhaust chemicals, and the resulting supply chain demands. While the U. S. Navy was interested in the laser as a shipboard weapon system the chemical laser provided too many hazards to the crew and ship, along with needing large storage areas for the chemicals [1].

At Stanford University, in 1971, J. M. J. Madey proposed the first FEL [2]. Madey combined multiple concepts such as undulators, optical resonators, and application of concepts from microwave tubes with atomic lasers to develop the FEL. These lasers use relativistic bunches of electrons, not bound within any medium, to create laser light. This allows them to achieve much higher power without having to worry about the effects on, or from, a medium. In addition, as an all-electric system, it provides a limitless (within the bounds of available fuel to run ship's generators) amount of ammunition for the laser, unlike the chemical laser. FELs are intrinsically broadly tunable in wavelength, and tend to scale to higher wall-plug efficiency at high power. Power output can be scaled in a variety of ways, by adjusting the peak electron beam current or the repetition rate between electron bunches. These advantages allow the overall output, power and wavelength, to be varied without having to alter the system construction.

High-power FELs may very well be the future for the U.S. Navy, providing an extremely efficient, reliable weapon system that operates at near the speed of light with a limitless supply of ammunition. FELs also have numerous opportunities in commercial industry, scientific research, and even space applications. There are some draw backs to FELs, the major two being the size and initial cost of the system, both of which are being researched to be reduced to a viable size and price for shipboard use. This includes optimizations of subsystems such as the electron beam sources. One design under consideration is the MK1 quarter-wave electron gun. This thesis will look at developing a cooling system for the copper cathode stalk used to hold and adjust the cathode inside the MK1's superconducting cavity.

Chapters II and III will discuss the components and theory of the free electron laser. This will provide an understanding of how all of the FEL pieces fit together, and how electrons can be used to generate a coherent beam of light as a usable laser beam. In

Chapter IV, the development of the MK1 quarter-wave gun will be examined, in addition, reasons for needing a cathode stalk cooling system will be discussed.

Chapter V discusses the design and construction of a cathode stalk test stand and cooling system, to include the design parameters and the computer simulations that led to the chosen design. Chapter VI discusses and compares the experimental results and makes recommendations for further designs and tests.

THIS PAGE INTENTIONALLY LEFT BLANK

# II. FREE ELECTRON LASER DESCRIPTION

An FEL generates electromagnetic radiation from a relativistic beam of electrons. The process the electrons go through and components they encounter from generation to laser generation to disposal, is described here.

There are two major types of FEL configurations, the oscillator and the amplifier. The designs share many of the same components, and are shown in Figure 1, a diagram of a recirculating energy recovery FEL. The major difference between amplifiers and oscillators is the extraction process of energy in the form of light from the FEL. The amplifier design amplifies an existing "seed" optical field; it relies on the electron beam energy being transferred to the light wave on a single pass through the undulator. The oscillator on the other hand is used in conjunction with several passes to generate the output beam. It is designed with an optical cavity that is enclosed by mirrors and contains an undulator in the middle. In both designs a small amount of electron energy on the order of 1–5% is transferred to the optical beam.

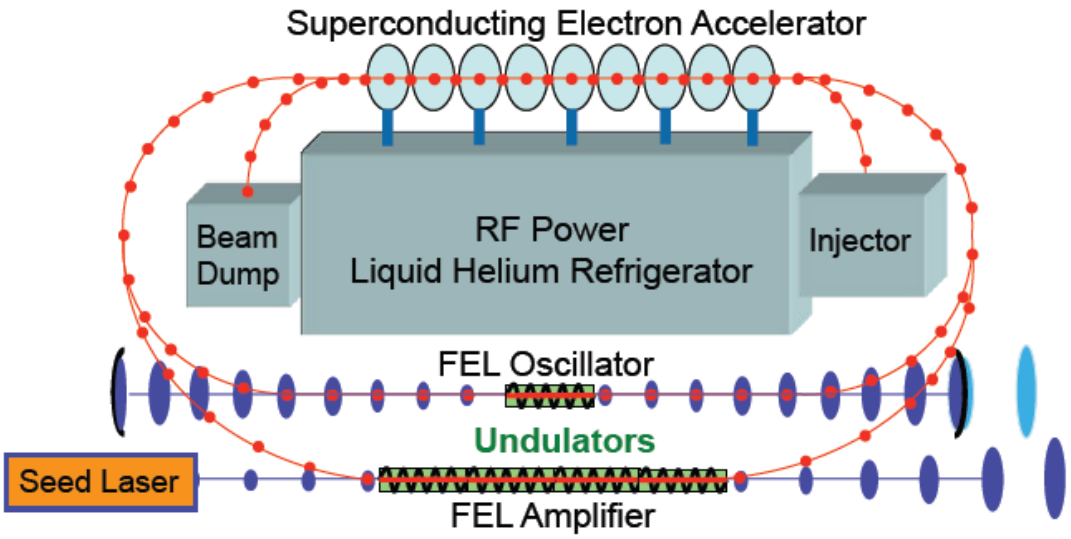


Figure 1. FEL Schematic (From [4]).

FEL beam generation and transport components include an injector, accelerator, undulator, resonator (for the oscillator design), seed laser (for an amplifier design), and beam dump. To shape and direct the electron beam focusing and bending magnets are used. The beam is transported within a vacuum enclosure, required both to prevent scattering of the electron beam and for the operating of the accelerator cavities. The following sections of this chapter will describe these components.

## A. INJECTOR

Electron beam creation begins with the injector. The injector is primarily made up of a cathode and an electron gun. The injector uses the cathode to produce a beam of electrons with a small spread in energy (velocity). There are three main types of cathodes, photocathodes, thermionic cathodes, and field emission cathodes. The photocathode uses the photoelectric effect with a pulsed drive laser of appropriate pulse length and energy to illuminate a cathode, thereby releasing electrons. The drive laser wavelength is chosen to overcome the work function of the cathode, allowing electrons to become free of the material. The drive laser also determines the electron pulse structure. Thermionic cathodes apply heat to a metal. Heat is added, increasing the thermal energy of the metal, until the energy of some of the electrons exceeds the work function, and the electrons are freed. Lastly, field emission cathodes rely upon geometry to create locations of high electric fields. The cathode is made up of tips, often pyramid shapes, where the electric field is enhanced. The field is enhanced so greatly at the field emitter tips that it allows the external field to be sufficiently strong to exceed the internal field that determines the work function, thus allowing the electrons to be "sucked out."

The electron gun provides the initial acceleration to electrons given off by the cathode. There are two principal types, direct current (DC) and radiofrequency (RF). Direct current guns are most often limited by achievable acceleration gradient, i.e., electric field, which can limit the charge per bunch of the electron pulses to less than 1 nC [3]. RF electron guns release electrons from the cathode and emit them into an RF cavity. The electrons can be accelerated in the RF cavity to higher energies (~5Mev)

prior to entering the linear accelerator, permitting a larger charge per bunch and a better beam quality. The RF gun is described in greater detail in Chapter IV.

FEL system performance is greatly affected by injector design, from cathode to gun choice. The goal is to produce an electron beam that is of the highest beam quality, and with the least variation in electron energies consistent with high charge per bunch. Reaching this goal will help the rest of the FEL system to radiate more efficiently and increase the overall power that can be extracted from the FEL.

## B. LINEAR ACCELERATOR

The superconducting radiofrequency (SRF) linear accelerator (LINAC) is the next component encountered by the electron beam. For this thesis, the focus will be on SRF accelerators, as that is the type to be used in the Innovative Navy Prototype (INP). The LINAC consists of several metal cavities that have external RF power supplied, creating strong electromagnetic fields within the cavities. The high voltage electromagnetic fields oscillate at the RF frequency and are synchronized to the electron beam pulses, allowing the electrons to gain energy over the course of the accelerator. This allows electrons entering the accelerator at 5 MeV to be accelerated up to relativistic energies of 100MeV after passing through ten cavities [4]. The relativistic voltages of the electrons are crucial to the generation of a laser from electrons. Figure 1 demonstrates the accelerator position in the FEL system, while Figure 2 shows a cut-away of an accelerator module.

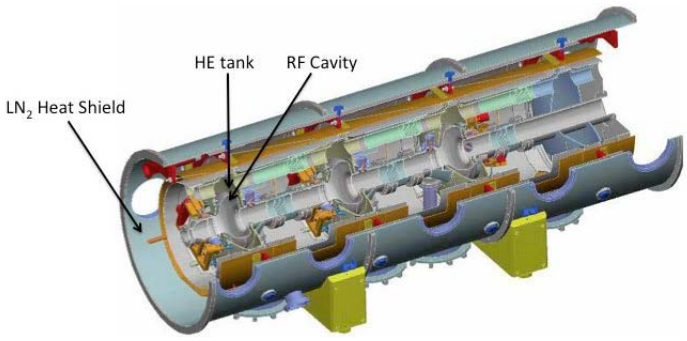


Figure 2. The accelerator is cooled with liquid helium to get the RF cavity to superconducting temperatures. A liquid nitrogen heat shield is used as a buffer from room temperatures to minimize the heat load on the helium (After [5]).

## C. UNDULATOR

Following the accelerator the electron beam will be directed into the undulator, which is made up of a series of powerful rare-earth magnets with alternating poles. This creates an alternating transverse magnetic field along the beam path. The strong Lorentz forces move the electrons back and forth, creating a "wiggling" motion. This wiggling causes the relativistic electrons to emit photons to form the laser beam, the theory behind this will be discussed further in Chapter III. There are two main types of undulators, helical and linear. In Figure 3, a design of a linear undulator is shown.

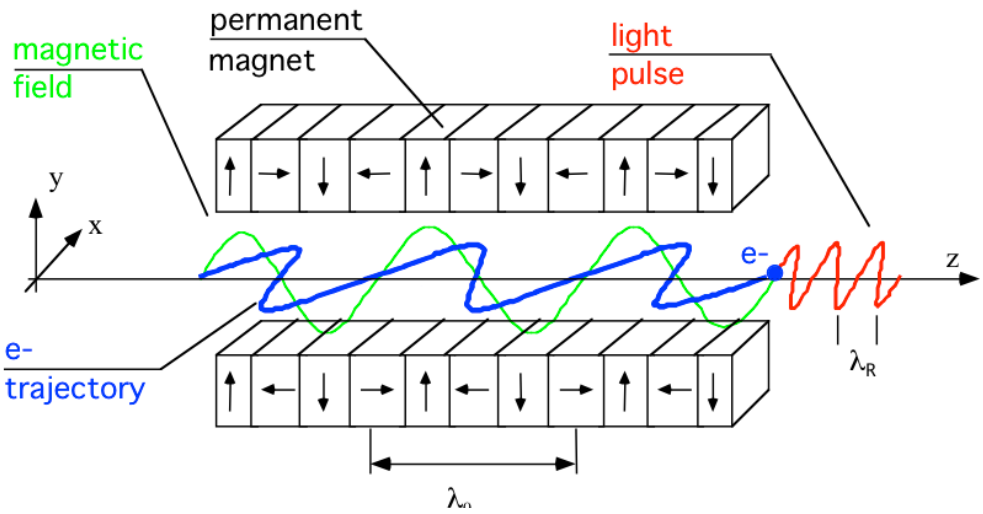


Figure 3. Schematic of linear undulator magnet orientation (From [6]).

## D. OPTICAL CAVITY

The optical cavity, or resonator, for an oscillator configuration contains the undulator. It also contains two mirrors; one at each end of the cavity surrounding the undulator. One of the mirrors is highly reflective, while the other is partially transmissive. An optical beam will travel down the undulator each pass and will hit the highly reflective mirror, then be redirected back through the undulator to the partially transmissive mirror. This reflection is timed with the electron beam pulses to create a continuous overlap throughout many passes, resulting in coherent amplification of the light beam, demonstrated in Figure 4. A fractional amount of this beam is transmitted through the transmissive mirror to the beam director and out from the ship as a laser

beam [4]. Amplifier FELs do not use this configuration, instead they use seed lasers in conjunction with the undulator to create the optical beam.

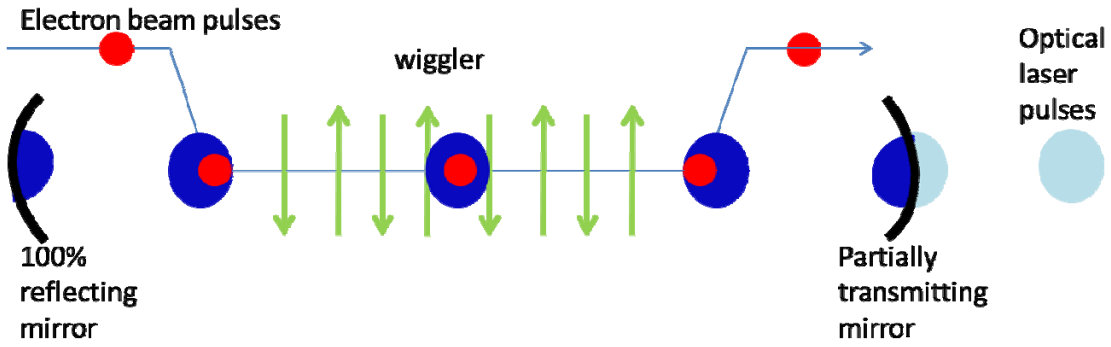


Figure 4. Optical cavity for oscillator FEL (After [4]).

## E. BEAM LINE SUPPORT COMPONENTS

Bending and focusing magnets are control components used to focus and guide the electron beam through the accelerator and FEL to ensure it follows the desired path. After the electron beam exits the accelerator it will enter a series of bending magnets used to direct the electron beam to the undulator. The focusing magnets focus the electron beam envelope transversely to the propagation axis. Bending and focusing magnets are analogous to prisms and lenses, respectively, in an optical system. Vacuum is maintained in the beam piping and components which also reduces electron scattering caused by particles. All of these components maintain and increase beam quality. The higher the beam quality the more able the beams will be to maintain more of their energy in a centrally focused manner, leading to an overall better beam entering the undulator.

## F. BEAM DUMP

High-power electron beams are being developed for shipboard use by the Navy. The laser only uses a small percentage of the power in the electron beam, leaving a large amount of power to be reclaimed. Reclaiming the power increases system efficiency, and reduces the amount of radiation emitted. In an energy-recovering LINAC (ERL) FEL the electrons leave the optical cavity and then are redirected back to the accelerator with the

bending magnets. The electrons enter the accelerator 180 degrees out of phase with the RF, allowing them to release energy to the RF field, and slowing the electrons back down to ~5 MeV [4]. The now decelerated beam is absorbed by the beam dump. The beam dump is a large block of absorbing material, such as graphite and copper, enclosed with shielding to prevent outside radiation, and equipped with cooling to manage heating. Since the electron beam has been slowed to less than 10 MeV it will not produce neutrons, and X-ray generation is significantly minimized, therefore the shielding requirements for shipboard use are greatly reduced.

# III. FREE ELECTRON LASER THEORY

There are critical differences between free electron lasers and conventional lasers. Conventional lasers require a lasing medium; this sets limits to the laser's power output (such as the amount of power the laser is able to produce due to concerns of medium heating) and typically allows for only specific wavelengths of operation. In the FEL the electrons are not contained within a medium allowing the user a tremendous amount of flexibility in power and wavelength. This chapter introduces the fundamental principles that create a laser from an electron beam.

## A. THE PENDULUM EQUATION AND RESONANCE CONDITION

Photons will be traveling through the undulator at the speed of light, *c*. Electrons are accelerated to relativistic speeds (slightly slower than *c*), and then enter the undulator. In this discussion a helical undulator will be assumed to simplify the mathematical expressions. First, a few parameters must be defined, starting with the normalized time $\tau$, which varies from 0 to 1 along the length, L, of the undulator. $\zeta$ is the phase of the electron, measured by the electron's relative position to a beam of electrons contained within one optical wavelength, $\lambda$. The rate of change of $\zeta$ is measured by the phase velocity, $\nu$. The frequency of the optical field is $\omega = kc = \frac{2\pi c}{\lambda}$. The optical wavelength $\lambda$ of the photon beam and the undulator period $\lambda_0$ have corresponding wavenumbers $k = \frac{2\pi}{\lambda}$ and $k_0 = \frac{2\pi}{\lambda_0}$. The principal motion of an electron through the undulator is in the z direction, $z(t) = \beta_z ct$. The normalized longitudinal electron velocity along this axis of the undulator is represented by $\nu_z$ and $\beta_z = \frac{\nu_z}{c}$. The coordinates are normalized using the following equations:

$$\tau = ct/L$$
$$\zeta = (k + k_0)z - \omega t$$
$$\nu = d\zeta/d\tau = L[(k + k_0)\beta_z - k] \quad (3.1).$$

The optical field amplitude, *a*, is another dimensionless parameter represented by

$$|a| = \frac{4\pi NeKLE}{(\gamma^2 mc^2)} \quad (3.2).$$

$\vec{\beta} = \frac{\vec{v}}{c}$ is the normalized velocity, the relativistic Lorentz factor is $\gamma = \left( \frac{1}{\sqrt{1 - v^2/c^2}} \right)$, *e* is the charge magnitude of the electron, and *m* is the mass of the electron. *N* represents the number of undulator periods, *K*, the undulator parameter, is a dimensionless measure of the field strength $K = \frac{eB_{rms}\lambda_0}{2\pi mc^2}$, and *E* the beam energy [7]. Strong or weak fields are related to the value of this optical field amplitude, if $|a| \leq \pi$, the optical field is weak and electrons do not "overbunch". If $|a| \gg \pi$, then the laser has strong optical fields where overbunching takes place [4]. Figure 5 shows the relationship between electrons and photons as a race through the undulator, where the red circles are the electrons, $\lambda_0$ is the undulator wavelength, and $\lambda$ is the optical wavelength.

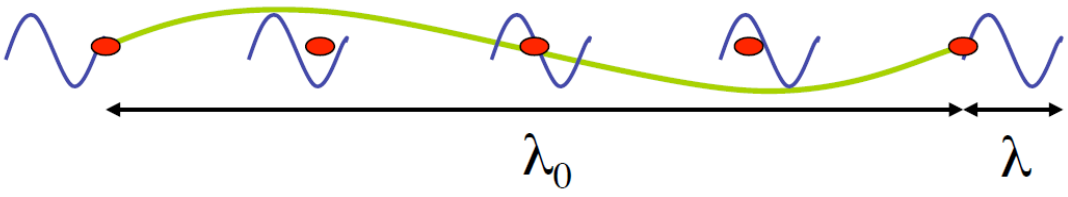


Figure 5. Electron-Photon interaction. Here the red circles are the electrons interacting with the optical wavelength, the blue waves, and the undulator wavelength, the green wave (From [4]).

The Lorentz force equations determine the motion of the electrons inside the helical undulator. As photons and electrons travel down the undulator, the photons will

overtake the electrons. As the electrons travel down the undulator they will interact with its magnetic field, as well as the optical field. $\vec{B}$ is the magnetic field strength and can be broken up into undulator and optical components. $\vec{E}$ is the optical electric field strength. These are defined as

$$\begin{aligned}
\vec{B}_{undulator} &= B(\cos(k_0 z), \sin(k_0 z), 0) \\
\vec{B}_{optical} &= E(\sin(\psi), \cos(\psi), 0) \\
\vec{E}_{optical} &= E(\cos(\psi), -\sin(\psi), 0) \\
\vec{B} &= \vec{B}_{undulator} + \vec{B}_{optical} \\
\psi &= kz - \omega t + \varphi
\end{aligned} \qquad (3.3)$$

The net force on the electrons from the net undulator and optical fields in the undulator is given by the relativistic Lorentz force equations:

$$\begin{aligned}
\frac{d(\gamma\vec{\beta})}{dt} &= -\frac{e}{mc}(\vec{E} + \vec{\beta} \times \vec{B}) \\
\frac{d\gamma}{dt} &= -\frac{e}{mc}\vec{\beta} \bullet \vec{E}
\end{aligned} \qquad (3.4)$$

where $\vec{v} = c\vec{\beta}$ is the electron velocity. We implicitly assume we can ignore space-charge forces. If we then substitute Equation (3.3) into (3.4) we find

$$\begin{aligned}
\frac{d(\gamma\beta_z)}{dt} &= -\frac{e}{mc}[E(\beta_x \cos\psi - \beta_y \sin\psi) + B(\beta_x \sin k_0 z - \beta_y \cos k_0 z)] \\
\frac{d(\gamma\vec{\beta}_\perp)}{dt} &= -\frac{e}{mc}[E(1-\beta_z)(\cos\psi, -\sin\psi, 0) + \beta_z B(-\sin k_0 z, \cos k_0 z, 0)] \\
\frac{d\gamma}{dt} &= -\frac{e}{mc}E[\beta_x \cos\psi - \beta_y \sin\psi]
\end{aligned} \qquad (3.5)$$

where $\vec{\beta}_\perp = \beta_x \hat{i} + \beta_y \hat{j}$. The transverse velocity $\vec{\beta}_\perp$ of the electron can be then be determined by integrating, giving Equation (3.6), assuming the relativistic electrons are traveling at approximately the speed of light, $\beta_z \approx 1$.

$$\vec{\beta}_\perp = -\frac{K}{\gamma}(\cos(k_0 z), \sin(k_0 z), 0) \qquad (3.6)$$

Therefore, the dimensionless transverse velocity $\beta_\perp$ can be represented as $\beta_\perp^2 = \frac{K^2}{\gamma^2}$.

The resonant wavelength, $\lambda$, is determined by the distance that a photon gets ahead of the electron in distance $\lambda_0$ and in time $\lambda_0 / \beta_z$. This leads to the resonance condition when one wavelength of light passes over an electron in one undulator wavelength [4].

$$\lambda = \frac{(1-\beta_z)\lambda_0}{\beta_z} \approx \frac{\lambda_0(1+K^2)}{2\gamma^2} \tag{3.7}.$$

A relationship between an electron's velocity and its energy is provided by the Lorentz factor as, and is used to determine the normalized velocity in the z direction $\beta_z$ [4].

$$\gamma^{-2} = 1-\beta_\perp^2-\beta_z^2,\ \beta_\perp^2 = \frac{K^2}{\gamma^2} \Rightarrow \beta_z \approx \frac{1-(1+K^2)}{2\gamma^2} \tag{3.8}.$$

The relationship between $\frac{d\beta}{dt}$ and $\frac{d\gamma}{dt}$ is established by taking the time derivative of (3.7) in (3.8).

$$\frac{\dot{\gamma}}{\gamma} = \frac{\gamma^2 \beta_z \dot{\beta}_z}{(1+K^2)} \tag{3.9}.$$

Taking the second time derivative of $\zeta(t)$ from (3.1) gives

$$\ddot{\zeta} = (k+k_0)c\dot{\beta}_z \quad (3.10).$$

Solving for $\dot{\beta}_z$ from (3.10), and substituting it into (3.9), the result is

$$\frac{\dot{\gamma}}{\gamma} = \frac{\gamma^2 \ddot{\zeta}}{\omega(1+K^2)} \tag{3.11}.$$

The resonance condition stated from (3.3) and microscopic electron motion $\dot{\gamma} = \frac{eKE}{\gamma mc}\cos(\zeta+\phi)$ can be substituted into (3.11) to give

$$\ddot{\zeta} = \frac{2\omega_0 eKE}{\gamma^2 mc}\cos(\zeta + \phi) \tag{3.12}$$

The dimensionless parameters given in (3.1) and (3.2) are used to simplify (3.12) to

$$\ddot{\zeta} = |a|\cos(\zeta + \phi), \tag{3.13}$$

which represents the microscopic electron motion in the form of the pendulum equation.

## B. OPTICAL WAVE EQUATION

The microscopic wiggling motion of an electron through the undulator, as described in the previous section, will generate and amplify light. The photons given off will create an optical field that interacts with the source current of the bunching electrons traveling through the undulator. Here the evolution of the light will be described by developing the wave equation.

The natural place to begin is with a derivation of the slowly-varying wave equation in the FEL interaction region where the current source is due to the bunching electron beam [8].

$$\left(\nabla^2 - \frac{\partial^2}{\partial t^2}\right)\vec{A}(\vec{x},t) = -\frac{4\pi}{c}\vec{J}_\perp(\vec{x},t), \tag{3.14}$$

where $\nabla = \hat{i}\partial/\partial x + \hat{j}\partial/\partial y + \hat{k}\partial/\partial z$, $\vec{A}$ is the optical potential vector, and $\vec{J}_\perp$ is the electron current. The electric and magnetic fields of the laser can be given by the optical potential vector. Assuming the coherent laser field is varying slowly compared to the optical frequency, $\omega = kc$, the optical potential vector for a helical undulator can be written as [8]

$$\vec{A}(\vec{x},t) = \frac{E(\vec{x},t)}{k}\hat{\varepsilon}e^{i\alpha} \tag{3.15}$$

where the polarization vector is $\varepsilon = (-i,1,0)$, the phase of the carrier wave is $\alpha = kz - \omega t$, and the laser's complex laser electric field is $E = |E|e^{i\theta}$. The wave's amplitude and phase

are assumed to be slowly varying along the axis of propagation (z axis). Utilizing this assumption, and substituting the simplified optical potential vector (3.15) into (3.14) the wave equation can be written as:

$$\frac{\vec{\varepsilon}e^{i\alpha}}{k}\left[\vec{\nabla}_{\perp}+2ik(\frac{\partial}{\partial z}+\frac{1}{c}\frac{\partial}{\partial t})\right]E=-\frac{4\pi}{c}\vec{J}_{\perp}(\vec{x},t)\,. \tag{3.16}$$

This equation can be simplified further by multiplying both sides by $k\hat{\varepsilon}e^{i\alpha}$, and by introducing "The Method of Characteristics," where $u=z-ct$, which will follow the light as it travels. The general wave equation can now be simplified into the parabolic or paraxial wave equation [7],

$$\left[\nabla_{\perp}^{2}+2ik\left(\frac{1}{c}\frac{\partial}{\partial t}\right)\right]E=-\frac{4\pi k}{c}\vec{J}_{\perp}\hat{\varepsilon}^{*}e^{-i\alpha}, \tag{3.17}$$

where $\nabla_{\perp}^{2}$ represents the transverse Laplacian $\nabla_{\perp}^{2}=\partial_{x}^{2}+\partial_{y}^{2}$, and an electron source current, $\vec{J}_{\perp}$, represents the total beam transverse current. The total beam current is the summation of all of the single-particle currents and is given by

$$\vec{J}_{\perp}=ec\sum_{i}\vec{\beta}_{\perp}\delta^{(3)}(\vec{x}-\vec{r}_{i}(t)), \tag{3.18}$$

where $\vec{\beta}_{\perp}$ is the electron's transverse motion, $\delta^{(3)}$ is the three-dimensional Dirac delta function, and $\vec{r}_{i}(t)$ is the trajectory of the *i*th electron.

$\vec{\beta}_{\perp}$ represents the transverse electron motion, as it contributes to the transvers current density, with

$$\vec{\beta}_{\perp}=-\frac{K}{\gamma}(\cos k_{0}z,\sin k_{0}z,0)=\mathrm{Re}\left(-\frac{K}{\gamma}i\hat{\varepsilon}e^{-ik_{0}z}\right) \tag{3.19}$$

The transverse electron motion (3.19) is then substituted into the current density (3.18). This new current density can be used in the parabolic wave equation (3.17) to obtain

$$\left[-\frac{iL}{2k}\nabla_{\perp}^{2}+\frac{\partial}{\partial\tau}\right]a(\vec{x},\tau)=-\left\langle je^{-i\zeta}\right\rangle_{(\vec{x},\tau)}, \tag{3.20}$$

where the dimensionless FEL current density is $j = 8\pi^2 Ne^2 K^2 L^2 \rho / \gamma_0^3 mc^2$, $\rho$ being the electron particle density. The dimensionless laser field is represented by $|a| = 4\pi NeKL|E| / \gamma_0^2 mc^2$, and < > is the average over the electrons in the beam.

Creating a dimensionless Laplacian operator allows further simplification of wave equation (3.20). Utilizing $\tilde{x} = x(k/2L)^{1/2}$ and $\tilde{y} = y(k/2L)^{1/2}$ as natural dimensionless coordinates, the new Laplacian can be represented by $\tilde{\nabla}_\perp^2 = \partial_{\tilde{x}}^2 + \partial_{\tilde{y}}^2$. Now we can write the dimensionless wave equation as [8]

$$\left[-\frac{i}{4}\tilde{\nabla}_\perp^2 + \frac{\partial}{\partial\tau}\right] a(\vec{r},\tau) = -\left\langle e^{-i\zeta}\right\rangle. \tag{3.21}$$

The left side of (3.21) describes the diffraction of the beam. When small diffraction exists, the $\nabla_\perp^2$ term is so small that (3.21) can be simplified to

$$\overset{\circ}{a} = -j\left\langle e^{-i\zeta}\right\rangle. \tag{3.22}$$

The average $\left\langle e^{-i\zeta}\right\rangle$ represents the amount of electron bunching, and the dimensionless current density, $j$, represents the measure of coupling between the optical and electron beams. There will be only a small coupling between the beams if $j < \pi$, but if $j \geq \pi$, then a large coupling is present. The rate of change in the optical field, $a$, is affected by both the average electron bunching and the dimensionless current. The evolution of $\zeta$ depends on the field $\overset{\circ}{a}$, creating a feedback loop that leads to the growth of the optical field. The optical field grows exponentially until it reaches saturation where the bunched electrons evolve further within phase space, and begin to take energy from the optical beam vice give energy to it [4].

## C. OPTICAL GAIN

The fractional gain of the optical beam power or energy is the optical gain. This can be determined by the total energy lost by the electron beam. Energy transfer occurs due to interactions between the optical beam and the electrons. The interactions between electrons and photons can be understood by examining the following two equations:

$$\begin{aligned} \overset{\circ}{a} &= -j\left\langle e^{-i\zeta}\right\rangle \\ \overset{\circ\circ}{\zeta} &= |a|\cos(\zeta+\phi). \end{aligned} \tag{3.23}$$

The dimensionless optical amplitude, $|a|$, determines strong or weak fields for FEL operations. If $|a|<\pi,$ the optical field is weak, if $|a|>\pi$, the optical field is strong. Here $\phi$ is defined as the optical phase.

In the case of weak fields $(a_0 \square\ \pi)$ and low gain $j<\pi$ $(|a|=a_0)$, the amplitude and phase evolution can be estimated. The power series expansion for $\zeta$ can be used to solve (3.22) for the lowest order change in the field and phase giving

$$\begin{aligned} |a(\tau)| &= a_0\left(1+j\left(\frac{2-2\cos(\nu_0\tau)-\nu_0\tau\sin(\nu_0\tau)}{2\nu_0^3}\right)\right)+\ldots \\ \phi(\tau) &= j\left(\frac{2\sin(\nu_0\tau)-\nu_0\tau(1+\cos(\nu_0\tau))}{2\nu_0^3}\right)+\ldots \end{aligned} \tag{3.24}$$

The initial phase velocity of the electron beam is represented by $\nu_0$. The gain in this region is

$$G(\tau)=j\left(\frac{2-\cos(\nu_0\tau)-\nu_0\tau\sin(\nu_0\tau)}{\nu_0^3}\right). \tag{3.25}$$

If $j\geq\pi$ and there are weak fields the gain from (3.24) and (3.25) changes, and can be estimated as

$$\begin{aligned} |a(\tau)| &\approx \frac{1}{3}a_0 e^{\left[\left(\frac{j}{2}\right)^{\frac{1}{3}}\sqrt{3}\left(\frac{1}{2}\right)\tau\right]}, \\ \phi(\tau) &\approx \left(\frac{1}{2}j\right)^{\frac{1}{3}}\frac{1}{2}\tau, \\ G(\tau) &\approx \frac{1}{9}e^{\left[\left(\frac{j}{2}\right)^{\frac{1}{3}}\sqrt{3}\tau\right]}. \end{aligned} \tag{3.26}$$

Figure 6 shows that there is electron bunching at resonance $(\nu_0 = 0)$, but as Figure 7 shows that with phase velocity slightly off resonance $(\nu_0 = 3)$ the gain can be significantly larger. In Figures 6–8, the electrons' initial and final positions through phase space are represented by the thin traces from the yellow dot (initial) to the blue dot (final). Changes along the vertical axis $(\nu)$ are related to the changes in electron energy $\Delta\nu = 4\pi N(\Delta\gamma/\gamma)$, where $\Delta\gamma/\gamma$ is the change in energy [4].

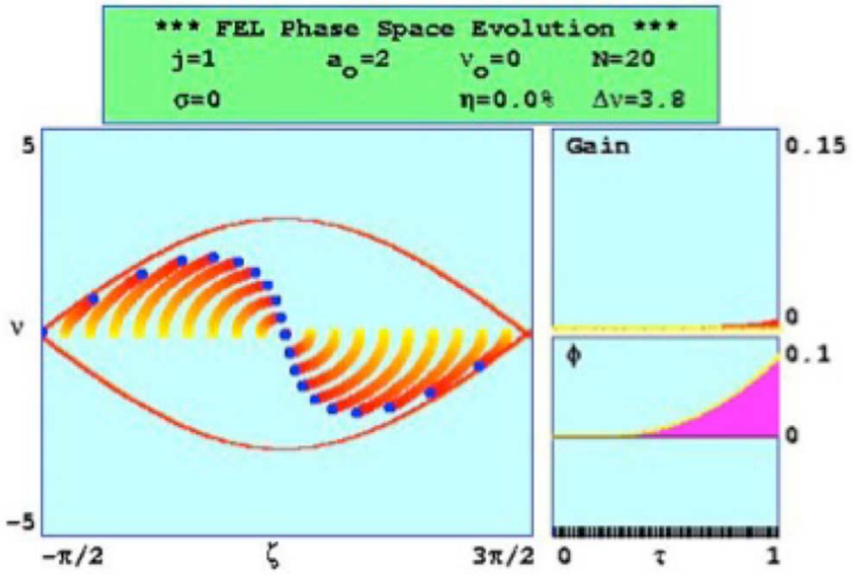


Figure 6. Electron Phase velocity at resonance (From [4]).

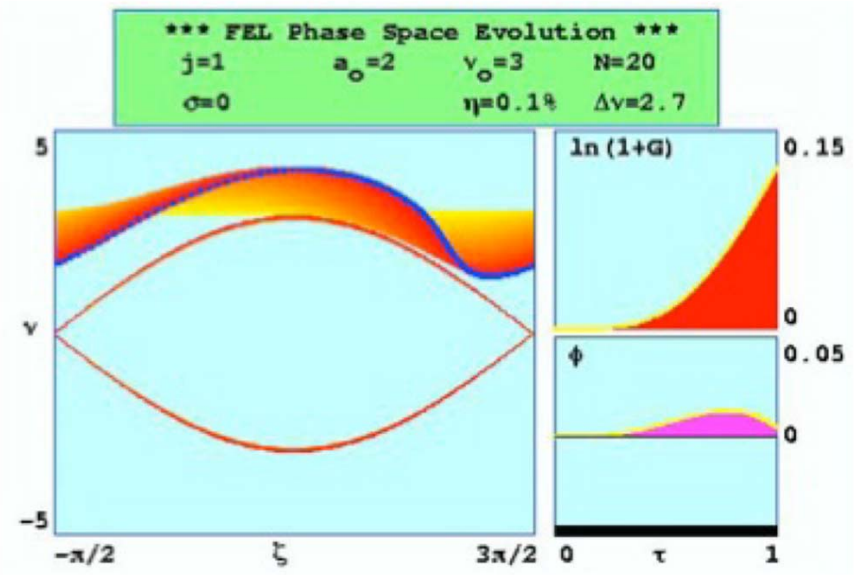


Figure 7. Electron phase velocity off-resonance (From [4]).

Over-bunching of electrons can occur for strong fields, $|a| \geq \pi$. In this case, the electrons are shifted from the proper phase for gain to one for absorption causing the gain to decrease significantly, demonstrated in Figure 8.

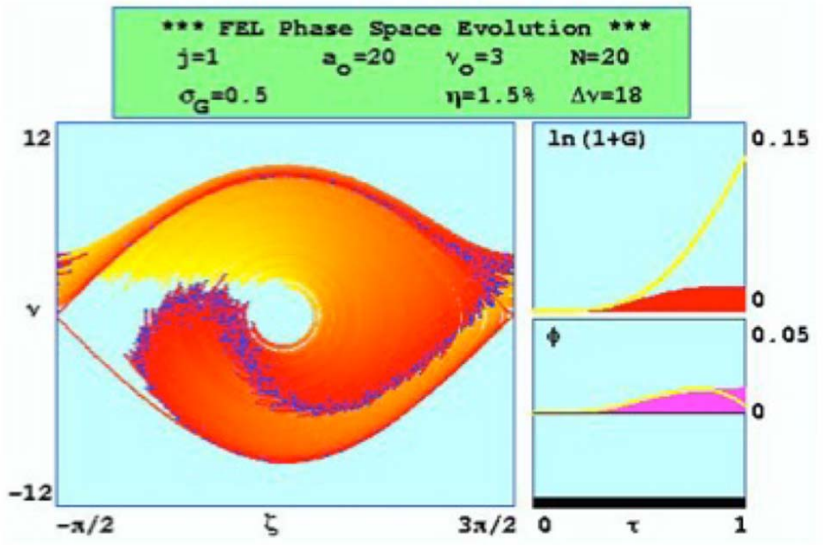


Figure 8. Strong optical fields (From [4]).

## D. BEAM QUALITY

For FEL theory to hold true there are limits on the angular spread and overall beam radius of the electron beam needed to fulfill the assumptions made above; in particular overlap in beam size and energy spread of the electron beam. Electron beam transverse quality is based on the divergence and size of the beam. This is quantified using the transverse emittance of the electron beam, $\varepsilon$.

$$\varepsilon = \sqrt{\langle x^2 \rangle \langle x'^2 \rangle - \langle x' \rangle^2} \approx r_b \theta_b \tag{3.27}$$

Here $x$ is the transverse position, $x'$ is the transverse velocity, $r_b$ is the radius of the beam at the waist, and $\theta_b$ is the far-field beam divergence. A normalized transverse emittance can also be defined as

$$\varepsilon_{normalized} = r_b \theta_b \gamma, \tag{3.28}$$

which is conserved as the beam is accelerated. Generally, the lower $\varepsilon$, the higher quality beam.

Another factor that determines the overall beam quality is the energy spread or phase velocity. A spread of phase velocities will result due to the finite spread of energies in a relativistic electron beam. This spread of energy impacts the FEL interaction as well as the transportation of the beam as it is accelerated, all affecting the effectiveness of the Free Electron Laser as a weapon. The limits on $\varepsilon$ and $\frac{\Delta\gamma}{\gamma}$ at the undulator can be propagated upstream to the electron beam source. One way to try to generate a beam that fits within these limitations is by creating an improved electron gun. This is the path taken by the NPS Beam Physics Lab (BPL) in the development of the MK I quarter-wave electron gun.

THIS PAGE INTENTIONALLY LEFT BLANK

# IV. DESIGN OF THE MK 1 SUPERCONDUCTING QUARTER-WAVE ELECTRON GUN

The electron gun is one of the major components that determine the maximum current and brightness that can be produced by an accelerator. DC and normal-conducting radio-frequency electron guns are the most popular for use in FELs today. While their technology is highly-developed due to the widespread usage and large amount of research that has gone into them, they still have significant constraints when operating in conditions requiring low emittance, high average power and high peak current, which are required to meet the FEL specification [10]. These limitations have led to the quest for a more effective electron gun, one of which is the superconducting electron gun. Among other advantages, shifting to a superconducting cavity significantly reduces dissipated RF power.

## A. GUN DESIGN

The first superconducting quarter-wave resonator electron gun was developed by the NPS BPL. Until its development the limited number of superconducting radio frequency (SRF) guns have all had elliptical cavity geometries [9]. The quarter-wave resonator geometry has multiple advantages over the previously-used elliptical cavity. These advantages include:

- a smaller cavity size for a 500MHz operating system
- the ability to operate at relatively low frequencies, and the reduced cost of utilizing low frequency RF sources
- reduced RF losses at the cathode, along with flexibility in how cathodes can be mounted in the gun
- an ability to operate at more relaxed cryoplant temperatures of ~4K while retaining compact cavities
- reduced wake field induced emittance growth and wake field losses
- allows for a smaller accelerating gap length compared to RF wavelength giving a higher transit-time factor, the net result is less sensitivity to exactly when the laser beam strikes the cathode [9], [10].

Originally, the cavity was developed as a booster for the Stanford Superconducting Accelerator (SCA) (which had been moved from Stanford and intended to be reassembled in a new configuration at NPS), but with the addition of a removable cathode stalk and a normal conducting (NC) cathode the cavity could be converted into an electron gun. The cavity was designed to have an operating frequency of 500MHz allowing for a beam injection rate of 100MHz into the SCA, while in gun operation the goal was the generation of a 1nC bunch accelerated to 1.2MeV [9].

Figure 9 shows a cross section of the cavity and cryostat together with the cathode stalk and cathode. Large grain niobium ingots were machined to create the end plates and "nose cone" of the cavity, while fine-grain rolled niobium was used to form the side walls. The niobium cavity has stainless steel flanges brazed onto each end, bolted to stainless steel piping, and is surrounded by a 6.8 L stainless steel liquid helium reservoir vessel [9]. Downstream of the cavity is a NbTi solenoid used for focusing and emittance compensation. Surrounding the liquid helium vessel and solenoid is a liquid nitrogen-cooled heat shield and multilayer insulation. Outside of these are a mu-metal magnetic shield and a low-carbon steel vacuum vessel. Vacuum is held between each of these layers.

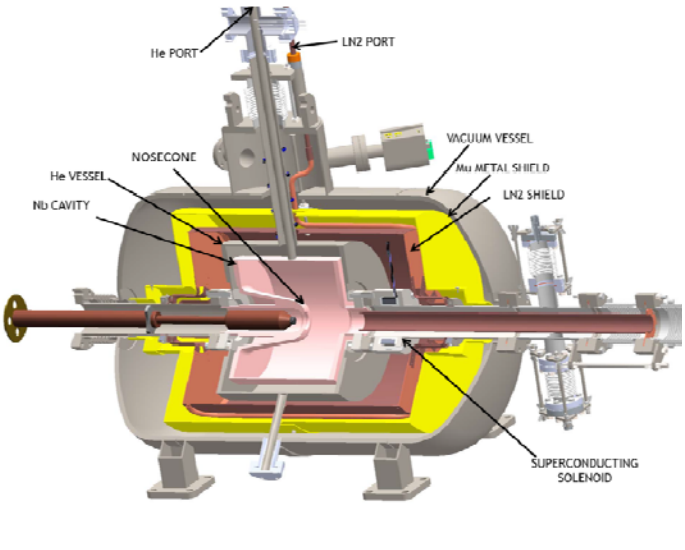


Figure 9. Cross section of the cavity with the coupler and cathode stalk installed (After [11]).

To transform the cavity from a booster to a gun a cathode stalk and cathode were added to the design. The stalk is a ~60 cm long hollow stalk made of copper. As it is essentially an antenna into the cavity, the parameters of the stalk were designed to minimize RF power dissipation and flow. The stalk has no direct physical contact with the cold cavity, reducing the heat flow into the cavity and the possibility of generating particulate contamination. However, this does allow for some of the RF power to flow out of the cavity and along the stalk [9]. Its length is optimized and has transitions in radius, to create impedance mismatches to minimize RF power flow into the normal conducting region. The cathode stalk is supported by a Teflon "spider" inside the pipe for centering and is attached to a mounting plate at the base of the stalk. The mounting plate is attached to the outer pipe and cryostat by bellows. The bellows are held in position by a series of screws that are also used to adjust the stalk's pitch, yaw, and axial position allowing the cathode position to be adjusted. This adjustment allows for changes in the transverse focusing and axial accelerating fields at the cathode tip, and it also changes the power coupling into the stalk region. This normal-conducting region is kept under vacuum with a dedicated pump [9]. There are also two capacitively coupled antennas mounted at the end of the stalk used to sense the power on the stalk. They can also be used to disrupt multipacting by injecting an RF signal.

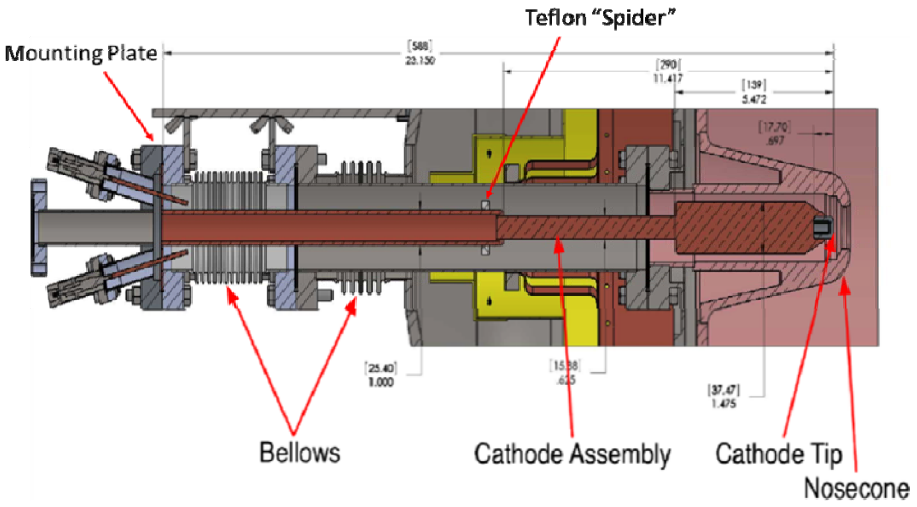


Figure 10. Detail of cathode stalk assembly with an inserted cathode (After [9]).

The cathode stalk is designed to easily change out cathodes. The cathodes are press-fit into the cathode stalk tip enabling testing of other materials and configurations. For initial testing a fine-grain normal-conducting niobium cathode was used to prevent contamination of the cavity. It was etched with buffed chemical polish, the same as the cavity, and press fit into the cathode stalk [9]. Figure 11 shows the cathode stalk machined by Niowave Inc., and a close up of the niobium cathode mounted to the tip.

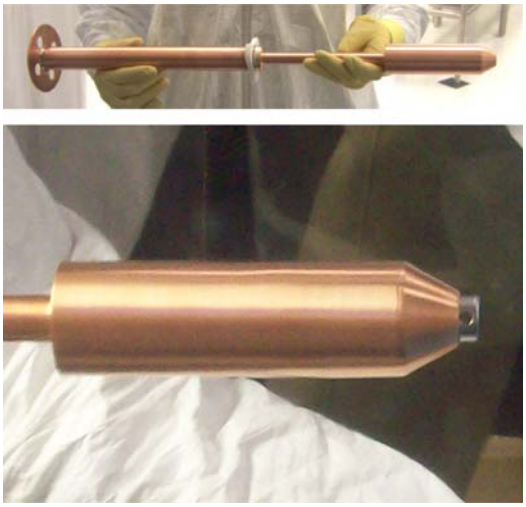

Figure 11. Top: Cathode stalk, without cathode, attached to mounting plate with Teflon spider in place Bottom: Detail of installed cathode on stalk tip (From [9]).

A cascade RF power coupler system was used for initial testing. The first stage is a coaxial coupler. The outer conductor is a stainless steel tube connected to the cryostat and cavity with an inner conductor that is a copper hollow tube (very similar to the cathode stalk), which can also be moved longitudinally to manipulate the coupling into the cavity. The accelerated electrons from the gun are directed through the hollow inner conductor. The second stage is a pair of capacitively coupled antennas similar to the ones used on the cathode stalk. These couple the RF energy into and out of the coaxial coupler [9].

The gun's RF source is driven by a reference oscillator (83.3 MHz) and frequency multiplier, which provides a 500 MHz input into the solid state amplifier (SSA) as well as providing the timing signal to the UV drive laser. This amplifier is capable of delivering

100W forward power to the cavity. The system can be easily upgraded to kW or higher power. A circulator is used to send the reflected power to a dummy load. A variable attenuator is installed before the amplifier to control the input power into the cavity while maintaining constant power for the laser timing and reference arm of the phase detection circuit. Figure 12 is a schematic demonstrating the flow of these components.

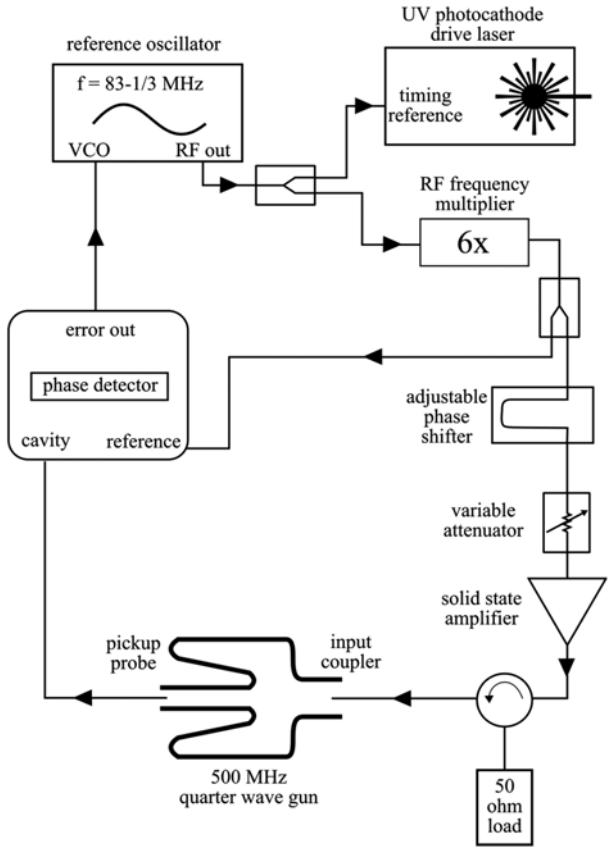


Figure 12. Schematic of the RF control circuit (From [9]).

A modified Coherent Elite DUO (generating 266nm light at nominal energy of 1mJ per pulse) laser is used to produce photoelectrons from the gun [9]. The laser beam diameter at the cathode can be adjusted using plates with 1 or 5 mm apertures that are inserted into the laser path. Without the plates the maximum laser diameter at the cathode is 10mm. The laser is directed through a vacuum window onto the cathode by a one square-inch aluminized fused silica mirror inside the beam line laser cross [9].

## B. INITIAL TESTING

Cryogenic testing was completed in two phases. The first was cavity operation without the cathode stalk. The cavity was cooled to ~4 K within two hours, and had a measured frequency shift from 500.3 MHz at room temperature to 501.0 MHz at cryogenic temperature. It had a static heat load of about 1.5 W, using approximately 2.1 L of helium per hour. Testing also showed that operating at temperatures lower than 4 K significantly improved the cavity quality factor ($Q$).

In the second phase of testing the cathode stalk and cathode were installed. Here the cavity temperature was maintained around 5 K (as indicated by the temperature sensor on the top of the cavity). The Coherent Elite DUO laser was used to generate beam from the Niobium cathode. Beam properties seemed unaffected by temperature changes below 6 K, but as the temperature approached 7 K the beam shape became distorted. Typical operation was at 10 W RF power to the cavity, and required ~14 L/hr of helium to maintain superconductivity temperatures around 5 K. Including overnight operations sustaining 5 K temperatures, an average of 250 L of helium was consumed per day. Overall the system operated quite reliably throughout six days of experiments, largely exceeding expectations. No fundamental limits were reached for bunch charge and beam energy, and the emittance measured is suitable for FEL operation in the infrared wavelengths as required by the NPS facility. More detailed experimental results are available in Ref [9].

## C. MOTIVATION FOR DEVELOPMENT OF A CATHODE STALK COOLING SYSTEM

The experimental results from the electron gun operation revealed that the consumption rate of helium from operation of the cavity without the cathode stalk to full operation as an electron gun significantly increased the rate of helium consumption from 2.1 L/hr to 14 L/hr. This increase is due to additional heating from the cathode stalk and NbTi solenoid operation, as well as RF losses on the cavity walls, and electron field emission. The solenoid was intended to be superconducting. It was attached to the liquid helium vessel with two copper bars, but the heat transfer was insufficient, once this is

corrected the heating will be much lower and mostly due to the cathode stalk and RF losses. There are multiple diagnostics throughout the gun, including temperature sensors on the cavity exterior walls, but currently there is no way to monitor the temperature on the cathode stalk, or at the cathode itself. While the stalk has no physical contact with the cold cavity, which reduces the heat flow into it, the significant increase in the heat load during full operation suggests the need to further analyze temperatures experienced at the cathode stalk, and search for a way to reduce the load on the helium cryostat.

While so far only operated at 10 W forward power the SSA is capable of delivering 100 W forward power to the cavity, which will in turn also be distributed along the stalk. Simulations and parameters determined by diagnostics already in the electron gun show that the electric and magnetic field is highest at the nose cone, which will also affect the temperature of the cathode stalk. Lastly, because of the open configuration and no choke cavity filter, some RF power flows out of the cavity affecting the temperature of the cathode stalk as well. All of these considerations have led to the need for a test stand to measure the temperature of the cathode stalk under similar circumstances, along with the ability to test different cooling systems to reduce the heat load that will be put on the helium cryostat.

THIS PAGE INTENTIONALLY LEFT BLANK

# V. CATHODE STALK TEST STAND AND COOLING SYSTEM DESIGN

As stated in Chapter IV, a test stand is needed to study the temperatures on the cathode stalk. It is also needed to develop an effective cooling system that will decrease the heat load carried by the helium cryostat. Excessive heat in the cryostat may cause the helium to boil, causing cavitation and vibration. In turn, this increases the cavity frequency jitter. This will also lead to quenching, taking the cavity from superconducting back to normal conducting. Also, while the BPL group is currently using niobium cathodes the intention is to use cesium telluride photocathodes in the future. Heat causes cesium to be "knocked off" of these cathodes shortening their lifespan. With the cathode stalk being cooled the cathode in turn will also be at lower temperatures, theoretically increasing its usable lifespan. The existing test stand will be used to study the effects of cryogenic temperatures on cathode lifetime and efficiency as part of another student's thesis work.

The goal of the cathode stalk test stand is to reproduce similar controllable conditions on the cathode stalk as occur in the MK I quarter-wave gun, and to measure the temperature effects of these conditions, as well as the ability to install and test cooling systems. This is the first time that a cooling system has operated in this kind of environment, and it was unknown how the cooling would affect the system. To begin with, we considered what additional data was needed from the test stand, for instance, shrinking and deflection of the copper stalk. We also needed to know how much cooling would be needed, if conduction cooling is enough, and the kind of flow rates needed to produce the desired effect.

## A. DETERMINING THE DESIGN

Options for a coolant were explored and liquid nitrogen (LN) was chosen. Water was ruled out because of potential freezing and behavior. If the MK I stopped operating while still being cooled the water would most likely freeze and expand. This could damage the stalk, and in extreme cases could cause the stalk to crack allowing for water

leaks into the cavity once it was brought back up to room temperature. This would incur time consuming and expensive cleanup, or ruin the MK I all together. Another coolant considered was low temperature helium gas, and in later testing this may be a viable way to cool the cathode stalk, but for initial testing the use of helium proved more complicated to use than the benefits it provided. Once the coolant was chosen a back-of-the-envelope calculation was performed using the heat capacity of liquid nitrogen to determine a rough estimate of the flow needed to cool the system receiving 100W of power to LN temperatures. The calculation indicated that approximately 12 mL/s of LN would be required to cool the system. Another requirement was the need for the coolant to leave the stalk at the same place it entered, preferably in some sort of piping to create an additional barrier against leaks.

Utilizing COMSOL, a multi-physics program, a simulation was created to determine where the maximum temperature would be located. The stalk was drawn in Rhino (a CAD program), then imported into COMSOL, where its inner surface was set to 77 K to simulate a LN bath. The numbers for the RF and laser heating were taken from a simulation executed in Superfish by Professor John W. Lewellen and applied separately to the stalk in COMSOL. The results from applying 100 W to the tip were as expected, with the highest temperature at the cathode at the tip of the stalk as can be seen in Figure 13.

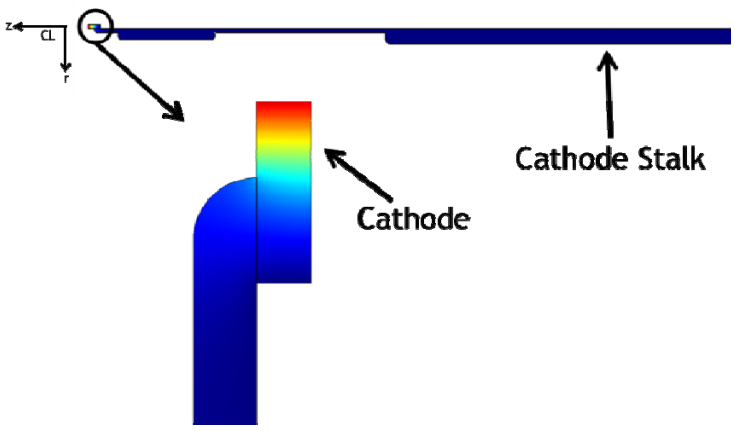


Figure 13. The top portion is a cut away of the cathode stalk with the cathode mounted on the tip. The maximum temperature is on the very tip of the stalk and is simulated to be 96.6 K. Dark blue is 77K.

The results given in COMSOL support concentrating the cooling at the tip of the cathode stalk. We decided on a helical design utilizing 1/8 inch copper tubing which has an inside diameter of 2 mm. We used COMSOL to model the flow, setting the inlet pressure to 50 psi with six turns in the helix. Figure 14 shows the results of this simulation. Although the COMSOL simulation showed the flow as being half of the required amount for cooling the stalk we decided to do a physical test of flow with water. The helix used in the experimental test had ten coils, as, after further discussion, this is what would be preferred for use in the cathode stalk due to the dimensions of the stalk. The experimental model was connected to a sink faucet, shown in Figure 14, where the pressure was measured to be approximately 60 psi. The flow from the helical tubing was measured to be roughly 20 ml/s, well over the flow needed for cooling the stalk. There were significant differences between the simulated and experimental data, this could be due to modeling errors. LN has a considerably lower viscosity than water, so this result is surprising, but is to our benefit. With this data in hand design of the test stand began, along with the first cooling system to be tested in it.

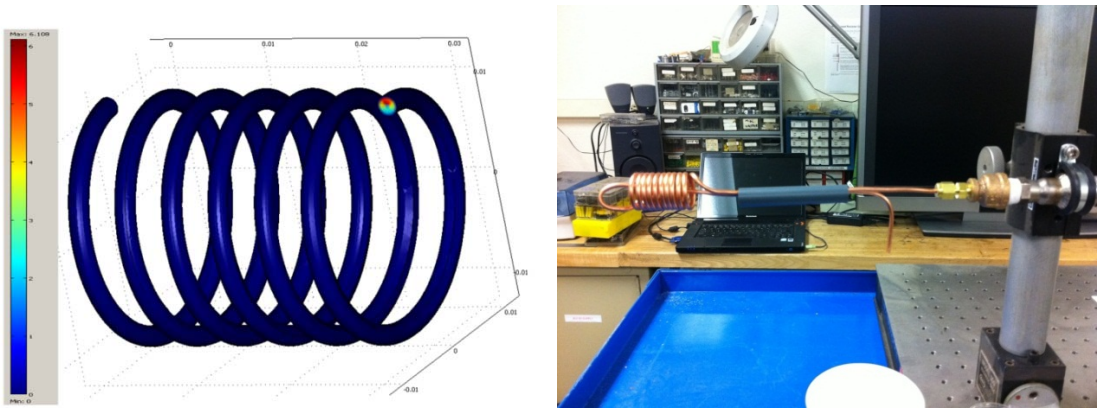

Figure 14. Left: COMSOL simulation of flow through 1/8" copper tubing, resulting in a maximum flow rate of 6.1 ml/s. Figure 14. Right: Set up used for experimental testing of the helical design with water.

## B. TEST STAND FABRICATION

A hollow copper stalk, similar to the parameters of the stalk used in the MK I, was designed in Rhino and fabricated by Don Snyder, as shown in Figures 15. The stalk

was created in 4 pieces that screw together. This was to enable easy change out of cooling systems, and also allow for the addition of a cathode at the tip.

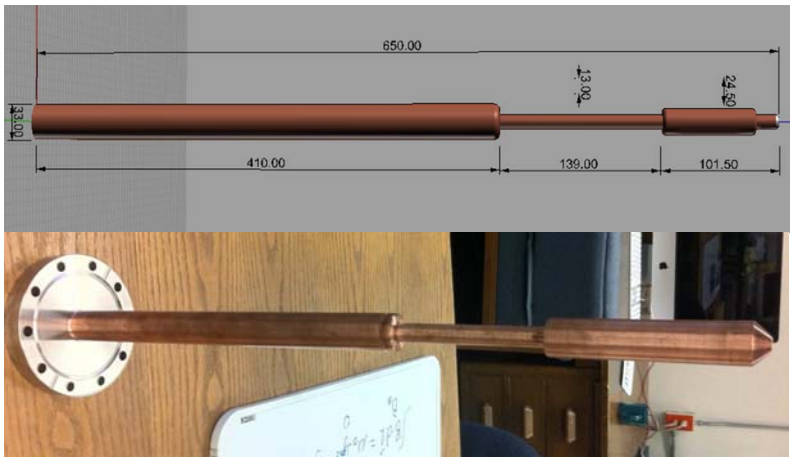


Figure 15. Top: Rhino model of test cathode stalk. Bottom: Completed test cathode stalk screwed into double sided flange used to mount into the test stand vacuum system. The stalk can be screwed apart at each place where it changes diameter as well as the tip.

The coil was also designed in Rhino, along with a vacuum chamber in which to mount the cathode stalk for testing, as shown in Figure 16.

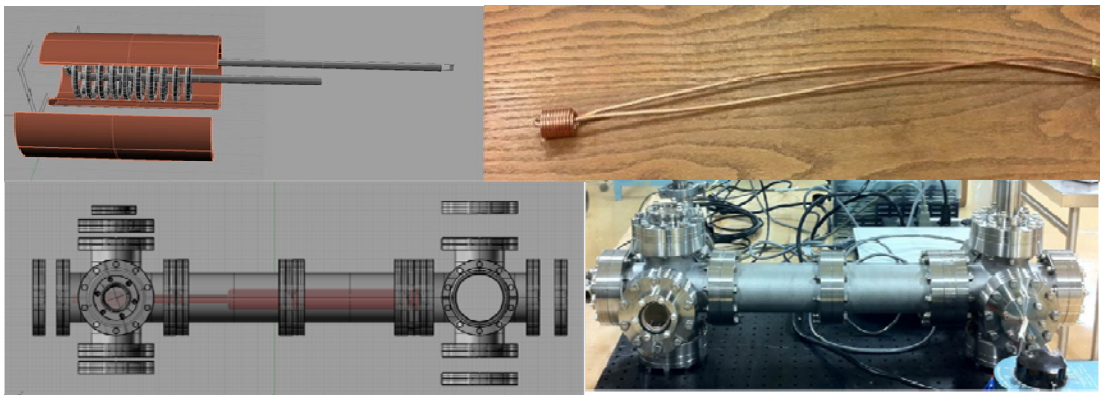

Figure 16. Top Left: Rhino design of cooling coil in cut-away view of the cathode stalk. Top Right: Fabricated cooling coil used in test stand. Bottom Left: Vacuum system designed in Rhino utilizing models of crosses and nipples from Lesker.com. Bottom Right: Assembled vacuum chamber test stand.

The coil has ten loops in the helix, starting in the middle of the length of tubing with one piece wrapping around the other going toward the end of the tubing. After the

tenth coil the tubing is straightened out parallel to the center piece. The helix has been coiled so that it will fit snugly inside of the cathode end of the stalk, with the top bend touching the screwed in cathode surrogate, and the coils along the walls of the first section of the stalk. To insert the coil into the stalk the tip was removed and the coil screwed down into the stalk. The two ends of the tubing protruding from the base of the stalk were to be attached to the coolant feed lines. The vacuum chamber was designed and built with 4-5/8 inch conflat flanges, allowing for the chamber to be directly mounted onto the MK I quarter-wave gun. This would allow for in-system testing to determine the actual effectiveness. Two six-way crosses were used, with two nipples and the blank flange supporting the stalk to make up the vacuum chamber. A third nipple may be used if a cathode is attached to the stalk to increase the range of the tip from the edge of the vacuum chamber. The blank flange came as a solid piece, and was machined with a threaded hole in the center to hold the cathode stalk. It also had three slots machined out to allow for good vacuum conductance, shown in Figure 17. Reducer flanges were used to mount windows, and feedthroughs for a power supply, fluid lines, and sensors, as well as cold cathode gauges to monitor vacuum pressure. Two windows were mounted at the cathode tip side of the stalk, one on top and one on the side, to allow for monitoring of any changes in the position of the stalk; in addition, they provide the ability to monitor cathode operations if the tip is replaced with a cathode. The vacuum pump and cold cathode gauge are both attached to the six-way cross at the tip of the stalk. Another window is at the cross at the base of the stalk, looking into the opening of the stalk. The six-way cross at the base also supports LN connections on the top, and the power feedthrough and sensor adapter on each side of the cross. These can be seen in Figure 18.

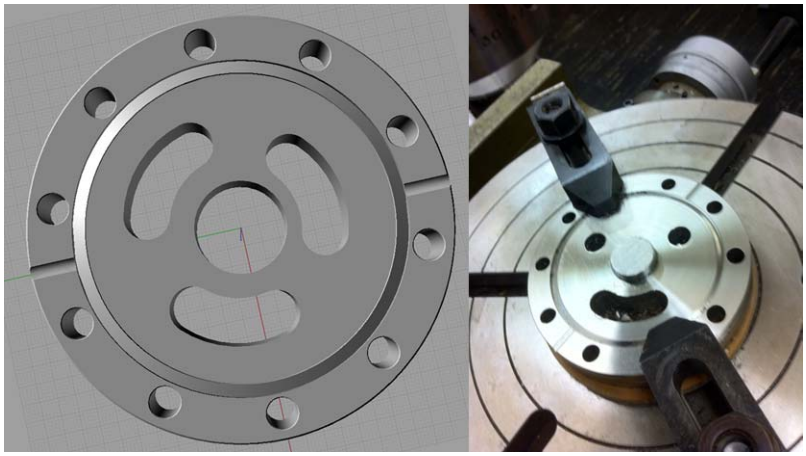

Figure 17. Left: Design of double sided flange in Rhino. Right: Double sided flange being machined for use in the vacuum system.

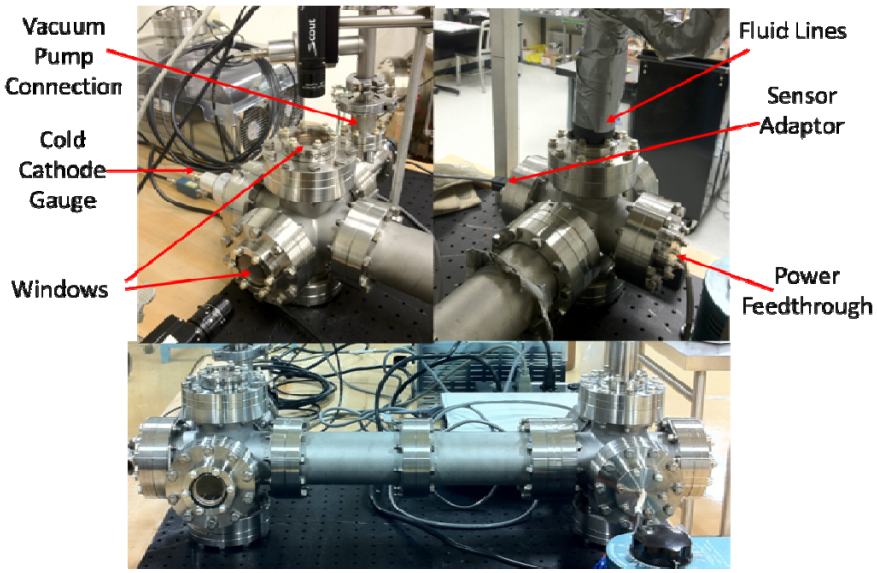


Figure 18. Test stand layout.

Once the cooling system and vacuum chamber were assembled the next step was to add the temperature sensors and heater cord to simulate the heating from RF power the stalk would receive in the MK I. The stalk was outfitted with four DT-670C-SD silicon temperature sensor diodes from Lake Shore Cryotronics. These diodes have a wide temperature range (from 1.4 K to 500 K) giving us the ability to test extremes and change cooling mediums without having to change temperature sensors. These are the same model of diodes used in the MK I electron gun, which will make eventual integration

easier. The diodes were soldered to 30 AWG Kapton wire to extend the leads. The Kapton wire is vacuum compatible and is also able to withstand temperatures over 500 K. One diode was mounted to the bottom of the of the stalk tip, prior to it being screwed onto the stalk, with Apiezon grease and a small piece of hard plastic that was screwed into the cap. The other three diodes were mounted along the outside of the stalk with Apiezon grease and zip ties as shown in Figure 19. The Apiezon grease is used to get good thermal contact between the diodes and the stalk.

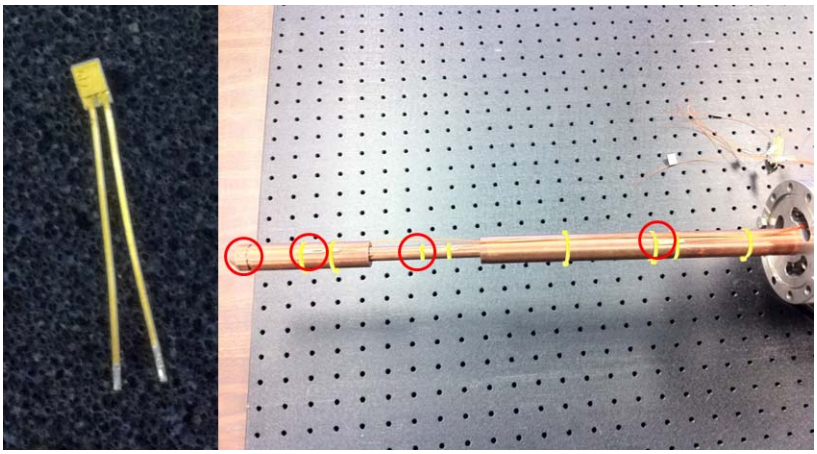

Figure 19. Left: DT-670C-SD diode. Right: Cathode stalk with mounted diodes. The circles indicate the location of the diodes, with the one at the tip of the stalk being inside of the stalk.

The leads were then soldered into a nine-pin type D subminiature feedthrough flange that is plugged into a Lake Shore temperature monitor. The monitor feeds the temperature readings into a LabVIEW program developed by Prof. Richard Swent which records the temperatures every five seconds and displays an hour plot of all four of the diode readings, as well as recording the data to disk. After the diodes were mounted the stalk was wrapped in OMEGA wraparound heating cord designed for small diameter objects. It is covered in a double-braided fiberglass outer sheath and operates up to 120 V, 260W. The cord is 12 feet long, and is wrapped around the stalk in its entirety, as can be seen in Figure 20, with turns per unit length being proportional to the fraction of heat expected to be deposited on the stalk in the MK I according to simulation. The cord was then connected to the power feedthrough which on the atmosphere side is attached to a

regular wall plug. This is used in conjunction with a Variac to adjust the wattage to 100W. The heater cord has a measured resistance of 58 Ω. When the Variac is set to 64 percent of 120 V output, it supplies a measured 76.3 V, providing 100 W of heat to the cathode stalk.

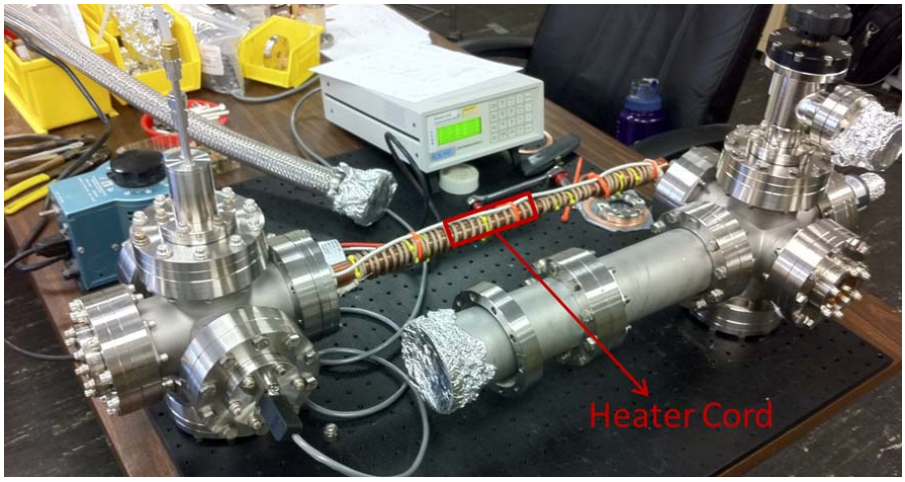


Figure 20. The cathode stalk is wrapped with the heating cord and being tested, in conjunction with the diodes, with the variac prior to completing the assembly of the vacuum chamber.

A fill-pot, built by Richard Swent and Mark Galt for the MK I, is used as a LN phase separator to provide more consistent LN flow to the cathode stalk cooling coil by eliminating or reducing gas bubbles. This allows the system to cool faster and stay cold more efficiently. The fill-pot is connected directly to the dewar through a solenoid valve controlled by an AMI Model 186 Liquid Level Controller. There is a sensor inside the fill-pot to determine the level of the liquid. The fill and stop fill levels are set by the user, and in turn are used by the controller to open and close the solenoid valve when these levels are reached. Initially, the cooling coil was connected to the bottom of the fill-pot using a gravity feed to flow the LN through the system. The return line on the cooling coil was connected to the fill-pot to recover any returning liquid, and gas is vented through tubing in the top of the fill-pot. Current operations have the fill-pot somewhat pressurized, and the cooling coil exhausting to atmosphere instead; this will be discussed more in Chapter VI. Figure 21 shows the fill-pot with the test stand.

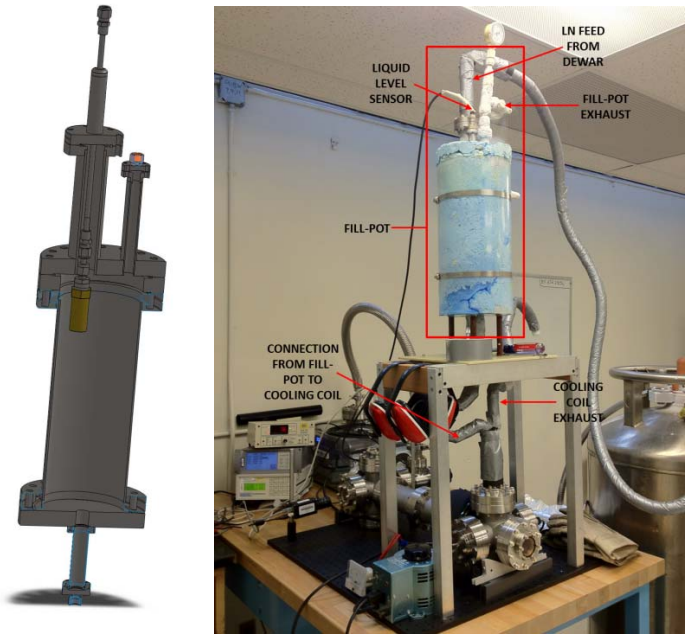


Figure 21. Left: Cut-away view of fill-pot (provided by Richard Swent). Right: The blue cylinder is the fill-pot. The dewar is connected to the top of the fill-pot, the cord connects the sensor to the liquid level controller. In this configuration the cooling coil exhausts to atmosphere.

Lastly, two cameras are mounted at both windows viewing the cathode tip. These positions can be seen in Figure 22. The cameras have high resolution and are connected to a computer operating through LabVIEW with a program designed by Richard Swent. The cameras are utilized to take pictures at different temperatures and compare them to determine bending and deflection in the cathode stalk.

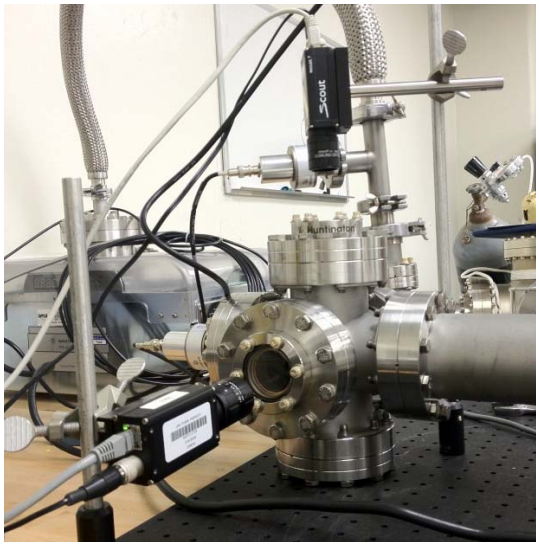


Figure 22. Cameras mounted to view tip of cathode stalk to record bending and deflection.

Since initial fabrication, changes have been made to the test stand to make it operate more efficiently. These will be discussed in the next chapter along with the results and findings.

# VI. CATHODE STALK TEST STAND EXPERIMENTAL RESULTS AND RECOMMENDATIONS FOR FURTHER TESTING

Broadly speaking, the cathode stalk was tested under three conditions: without cooling of any sort other than conduction; with water cooling; and with liquid nitrogen cooling. To make interpretation of these results easier to read we first introduce some nomenclature. The temperature measurement diodes along the stalk will be referred to as T1, T2, T3, and T4, and represent the temperatures along the stalk, starting from the tip of the stalk, as shown in Figure 23. Recall that T1 is on the inside of the stalk just under the tip cap, while diodes T2-T4 are on the exterior of the stalk. Temperatures were measured on the vacuum housing as well with a thermal camera. These temperatures will be referred to as HT1, HT2 and HT3, again started at the location of the stalk tip and progressing to the end. The position of these temperatures can be seen in Figure 23 as well.

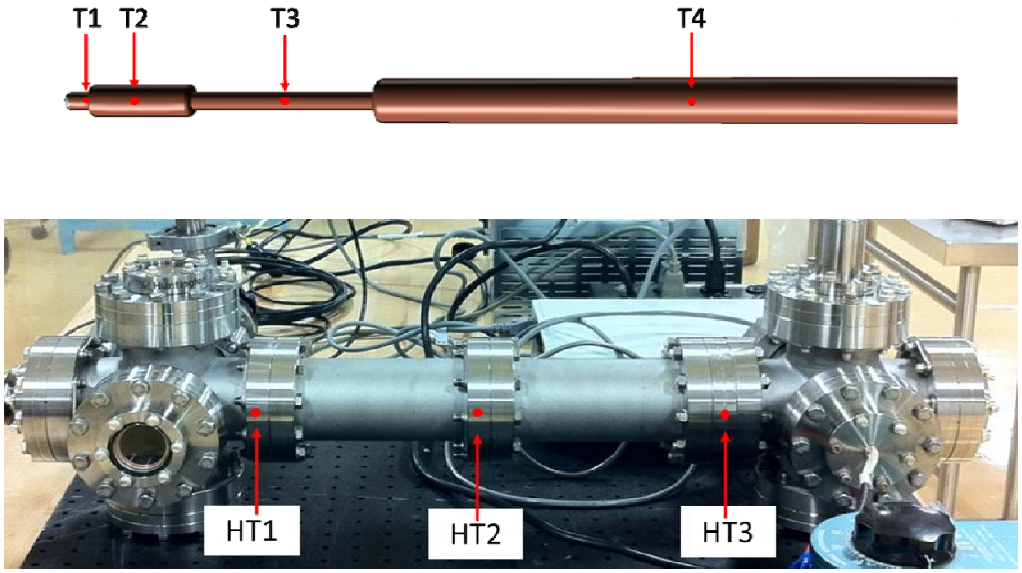


Figure 23. Top: Illustration of temperature sensor diodes locations, T1 being inside of the cap at this position. Bottom: Spots where thermal camera was focused to obtain temperature. Note, HT3 is on the mounting flange connected directly to the cathode stalk.

## A. INITIAL TESTS

The cathode stalk was initially tested with no cooling. The vacuum chamber was pumped down and holding steady at $3.7x10^{-5}$ Torr, and all four temperature sensors were reading from 292–293 K. Power was slowly applied utilizing the Variac. The slow transition was for two reasons: to obtain an estimated equilibrium temperature at several applied power settings: and to allow the vacuum chamber and stalk to "bake out" gradually as the various materials were heated. The Variac was raised in ten percent (of 120 V) increments up to 50 percent, and then in five percent increments until reaching 64 percent, corresponding to 100 W applied to the cathode stalk. The power was maintained at each step until the temperature reached a steady state. The results are shown in Figure 24. The final temperatures at the tip of the stalk (those having the most effect on the cavity) for 100W were T1 = 439.4 K and T2 = 439.4 K. The heat load was then calculated to determine the load it would place on the helium cryostat utilizing [12]

$$\dot{q}_{\text{net 1 to 2}} = \frac{\sigma(T_1^4 - T_2^4)}{\frac{1}{\varepsilon_1} + \frac{1}{\varepsilon_2} - 1}$$

$$P = \dot{q} A \quad ,$$

where $\sigma = 5.67 \times 10^{-8}$ W/m$^2$K$^4$ is the Stefan-Boltzmann constant, $A$ is the area of the stalk adjacent to the superconducting cavity, and $\varepsilon$ is the emissivity of the stalk (cavity wall). The area was estimated based on the amount of the stalk in the nose cone, at 12 cm length, with the radius in this section being 1.27 cm. The emissivity of niobium at room temperature is estimated to be 0.374 [13]. The emissivity of copper is highly dependent on the extent of polishing and the amount of oxidation on the metal, and can range from 0.015 – 0.78. Emissivity in copper goes up with oxidation, and the stalk in the MK I will be polished, so here a range of numbers from 0.05-0.2 will be used for the emissivity to get a range of $\dot{q}$. $T_1$ is the temperature of the stalk that will be located in the nosecone (T1 and T2 in Figure 23) measured to be 439.4 K, and $T_2$ is the temperature of the niobium cavity, 4.2 K. The active heat load on the helium cryostat from the cavity alone (when operated at the maximum accelerating field) is ~10 W. With no cooling, an

additional heat load from the cathode stalk can be anywhere from 0.93–3.02 W, depending on the actual emissivities of the niobium and copper, which is about a 10–30% increase of the active heat load on the cryostat. To put this into perspective, the passive heat load of the cryostat (e.g., with no accelerating field in the cavity) is approximately 2 W and requires 50 L per day of LHe to maintain the cavity at 4.2 K.

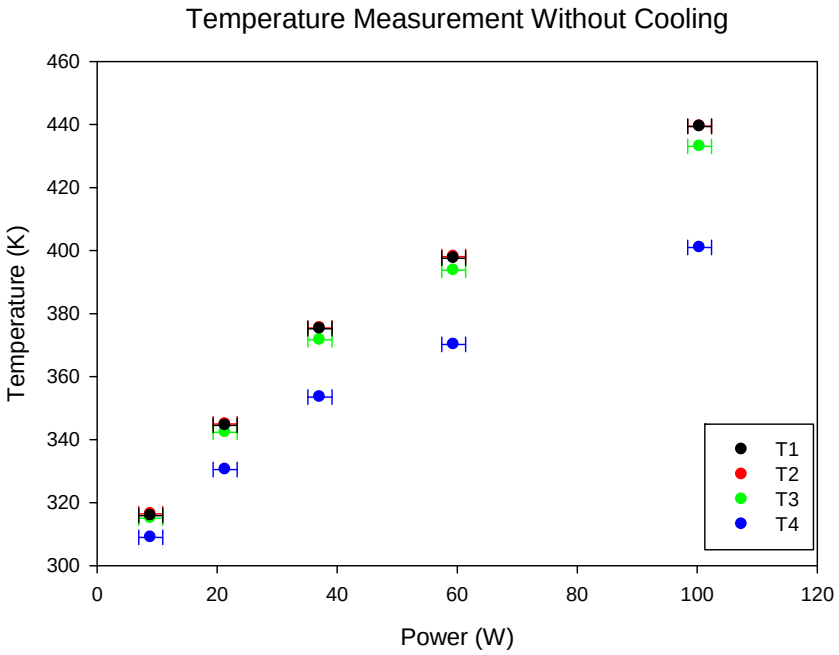


Figure 24. Plot of temperatures taken as applied power was increased, with error bars of 2 W. This data was taken prior to the LabVIEW program being established.

During this first test the vacuum chamber was "baked out," and an increase in voltage also increased the vacuum pressure in the chamber. In particular, materials which have not previously had heat applied when under vacuum (such as the heater tape) tend to release large amounts of gas under these conditions, and can raise the pressure in the chamber significantly. Once the heat had driven off all of the gas the pressures dropped back down. This can be clearly seen in Figure 25. The temperature of the vacuum chamber was also taken with a FLIR Thermatrak camera at the positions

illustrated in Figure 23. HT1 and HT3 were measured to be 307 K, and HT2 was 309 K. The middle of each of the nipples, were also measured with a temperature of 323 K.

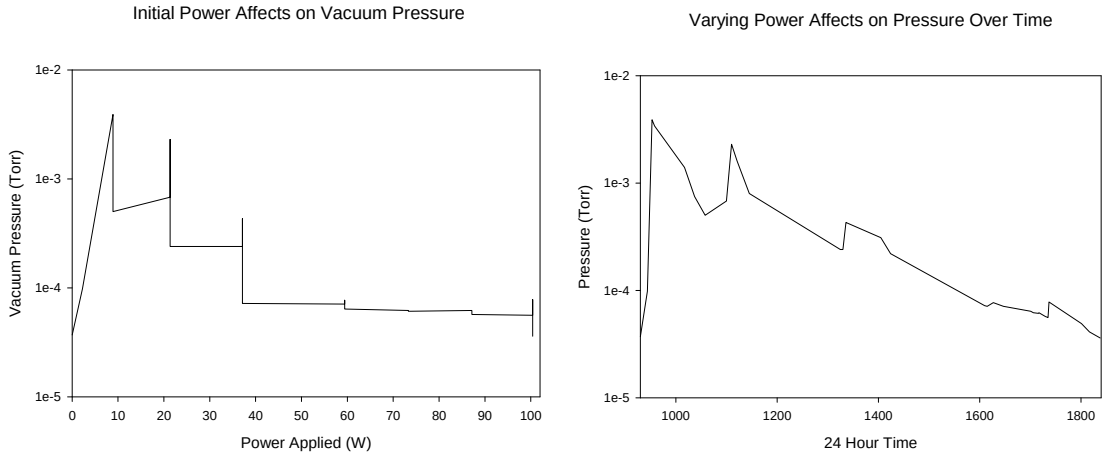


Figure 25. Left: Demonstrates the pressure increases and drops over the duration of the applied power. Right: Plots the pressure change over time, better representing the pressure rise and decrease.

The cooling system was then tested with a water chiller, which was easier to establish basic operation with than an $LN_2$-based system. A NESLAB ThermoFlex1400 was used to feed 283 K water into the cooling coil through the fluid feeds at 48 psi. The chiller was set up in the evening, with the stalk temperatures at a room temperature of 293 K, and left on overnight to ensure a steady temperature prior to adding power. The cooling system worked optimally overnight with temperatures ranging from 284–289 K. The 289 K reading was at T4, where a higher temperature was to be expected due to the flange the stalk was mounted to being, generally, at room temperature. Power was applied in ten percent (of 120V) increments up to 50 percent and then increased to 64 percent for a total of ~100 W. The chiller was able to maintain relatively stable temperatures with the least increase in temperature at the front portion of the stalk where the cooling coil is located. The temperature at T1 and T2 steadied out at ~289K with 100 W applied. T3 and T4 were significantly higher at 318 K and 344 K, respectively, as was expected due to the limited amount of cooling in these portions of the stalk. Figure 26 shows the progression of the temperatures varying with power and with time. After

the operability of the test stand was verified with cooling water the next step was to blow out the water with high pressure air and shift the cooling medium to LN.

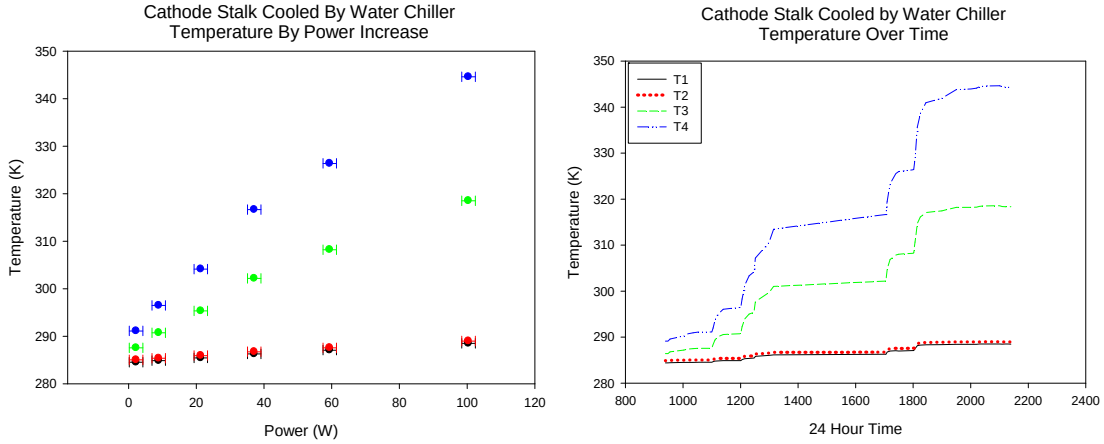


Figure 26. The test stand is operating as expected, with temperatures T3 and T4 higher than the front of the stalk. T1 and T2 offer promising results in this initial phase.

## B. TESTING WITH LIQUID NITROGEN

### 1. Initial Configuration

The test stand was connected to the fill-pot (as shown in Appendix C) and the fill-pot input was connected to a LN dewar through a solenoid valve. The liquid level controller was set to open the solenoid valve when the fill-pot level was at 0.7 inches and close when the level reached 6.5 inches. A leak from the valve controller body became apparent upon opening the liquid valve on the dewar. After multiple attempts to tighten the valve it was removed and a hairline defect or scratch running across the threads of the valve body was discovered and taken to be the most likely source of the leak. The dewar was then connected directly to the fill-pot and controlled manually from the tank valve, while still using the fill-pot liquid level monitor to judge when to open and close the dewar. The initial temperatures on the cathode stalk were at room temperature (from 293–294 K), and vacuum was maintained at a pressure of $\sim 10^{-6}$ Torr. For the initial cooling test with the fill-pot, the dewar was opened at 1050 to begin fill of the fill-pot. Temperatures on the cathode stalk did not begin to drop until 1120, and finally bottomed

out at 1339 with T1=244.1 K, T2=244.7 K, T3 = 253.7, T4 = 271.3. After 1339 the temperature began to increase. This is suspected to be because of a lack of differential pressure between the cooling coil input and exhaust to maintain a strong enough flow to continue cooling the system. Figure 27 shows the progression of the temperatures over time. There are fluctuations at various intervals; these are due to filling the fill-pot. The pressure from the open dewar increases the flow rate of the LN flowing through the cooling coil causing the temperature to drop more drastically, but would then lower the fill-pot level and the amount of LN going into the coil. It could be seen that the more full the fill-pot, the more significantly the temperature would drop. The results from the first test showed that this configuration would not provide substantial enough cooling for the cathode stalk while operating in the MK I and that a pressurized system would be necessary.

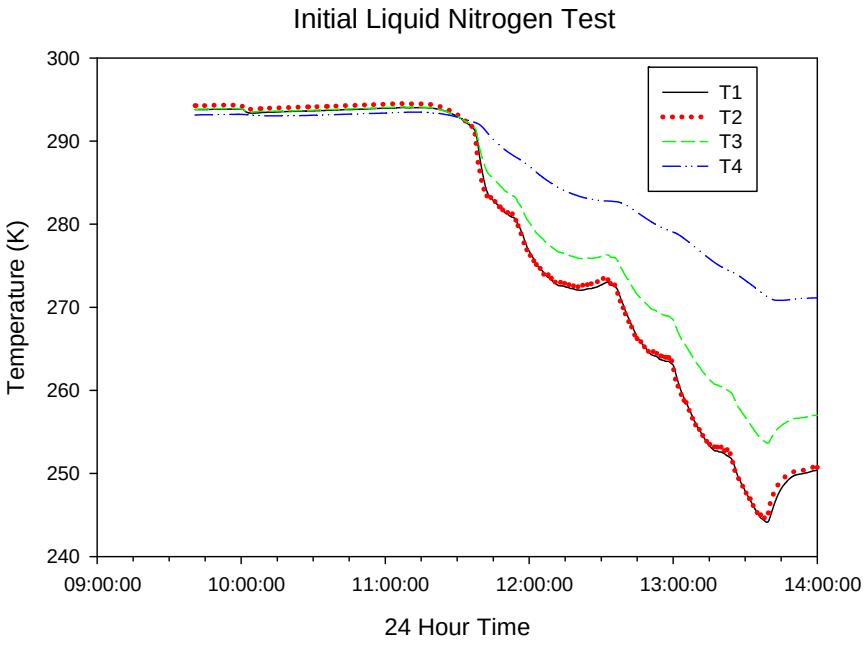


Figure 27. First attempt at cooling the cathode stalk beginning at room temperature with no heat applied. Pressure from opening the valve on the LN tank to fill the fill-pot had significant effects on the temperature, as did the amount of LN in the fill-pot.

### 2. $LN_2$ Fill System Modifications

The system was reconfigured to allow an increased differential pressure across the cathode cooling loop. The fill-pot was fitted with a pressure regulator valve on its exhaust, and a pressure gauge. The return line from the cooling coil was removed from the fill-pot and allowed to exhaust to atmosphere, while the return connection on the fill-pot was plugged to create a pressure differential. On the first test the regulator valve did not operate as intended, and did not maintain any pressure. To correct this, a plug was used in the regulator valve and it was operated manually, along with the filling of the fill-pot from the dewar. The plug was removed while filling the fill-pot, to allow gas to vent, and then immediately replaced once the LN tank valve was closed. Figure 28 shows a plot of stalk temperatures vs. time for this test. The LN tank valve was opened at 1454 for the initial fill. It was only partially opened to control the flow going into the fill-pot. At 1527 the temperatures began to increase, so the LN tank valve was fully opened. The temperatures recovered and then began to decrease again; these changes can be seen in Figure 28. The stalk hit minimum temperatures at 1605, these temperatures were T1=91.4 K, T2=88.2 K, T3=126.4 K, and T4=198.1 K. The stalk remained cool with steady temperatures until the LN was stopped at 2145. This time the temperatures reached lower minimums much more quickly. Instead of almost three hours to reach a minimum during the initial test, following the modifications it took approximately an hour and ten minutes. The results from this test were much more favorable than the initial LN test. Next power was added to the cathode stalk to determine the cooling abilities of the system.

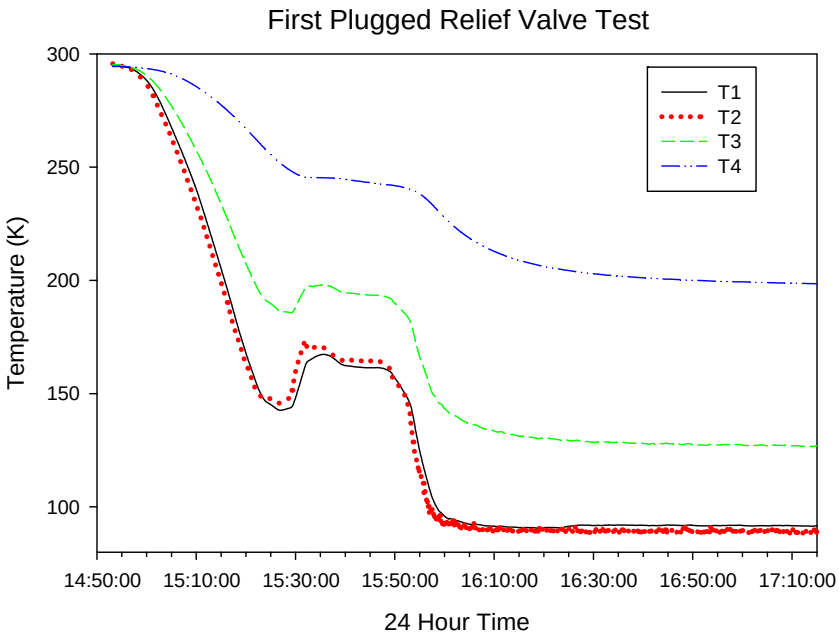


Figure 28. Test of cooling system without heat using a modified regulator valve. All temperatures readings are as expected with T4 being the highest due to its connection to the flange, and thus the outside world.

Prior to the next cool down the supporting flange for the cathode stalk was wrapped in thermal insulation in hopes that it would help reduce the effects of the outside temperature on the end of the stalk. T1 and T2 reached minimum temperatures in approximately two hours while T4 continued to slowly decrease for another three hours. The steady minimum temperatures were T1=90.5 K, T2=90.6 K, T3=124.5 K, T4=186.7 K. The extra insulation decreased the temperature in T4 by ~10 K. At 1442 the variac was turned on to ten percent of 120 V, equivalent to 2.2 W. After 20 minutes the voltage was increased by 20 percent and then increased by ten percent every ten minutes up to 60 percent, about 87 W. The Variac was left at 60 percent until the temperatures became steady, which required about three hours. During this period, towards the end of the three hours there was an approximately 20 minute period where the temperature spiked, and then dropped back down. The cause of this anomaly is thought to be a gas bubble trapped in the cooling coils, but that has yet to be confirmed. The steady temperatures at 60 percent heater power (87 W) were T1=176.0 K, T2=184.2 K, T3=238.2 K, T4=305.3. Temperature ranges from cool down to power application can be seen in Figure 29.

Using the temperature from T2, and an emissivity of 0.1 for copper, the heat load on the cryostat was calculated to be 0.05 W. In comparison to the 1.7 W calculated for the stalk with heat only, this is a 97% decrease, and instead of requiring 50 or more liters of helium a day just to counteract the heat from the stalk, it would only require an additional 1.5 L per day.

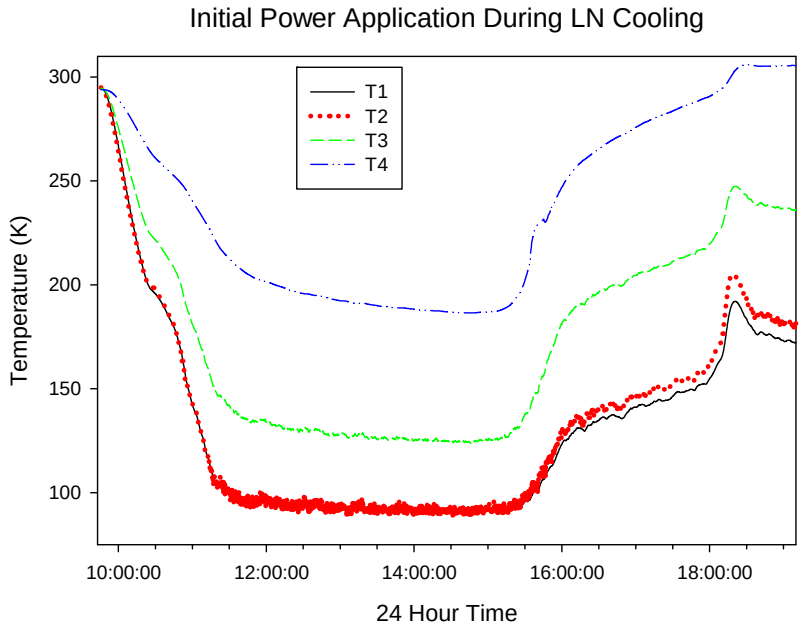


Figure 29. Plot of cooling from room temperature to steady state, and then the gradual addition of power, stopping at 87 W. Temperature reached equilibrium at ~1844.

The experiment was repeated and the apparatus improved over the next few days. One of the improvements was to fill the fill-pot sooner, a nominal fill level of four inches was chosen for this configuration, and a stop fill level at 8.5 inches. This ensured that the fill-pot was never empty; at a lower start-fill level, the increased pressure during the start of filling could force all of the remaining liquid nitrogen through the cooling loop. Increasing the start and stop fill levels greatly improved the cooling rate of the stalk. T2 took approximately eight minutes reach its minimum temperature and T1 took ~20 minutes. Regardless of configuration during manual operation, T4 consistently takes the longest to stabilize, reaching its minimum after about three hours of cooling.

Another modification to the experiment consisted of applying a full 100 W to the stalk in a step-function turn-on, instead of gradually adding power to the stalk. This is a more accurate reproduction of the effects that would be felt in the MK I. The results of this test are promising. The best case scenario can be seen in Figure 30. With 100 W applied the equilibrium temperatures were T1=92.1 K, T2=94.1 K, T3=164.7 K, and T4=270.9. This equates to 0.003 W, or an additional 0.1 L of helium per day to cool the heat added by the cathode stalk. The average T2 temperature seen in this configuration is 112 K, which equates to 0.007 W or 0.2 L/day.

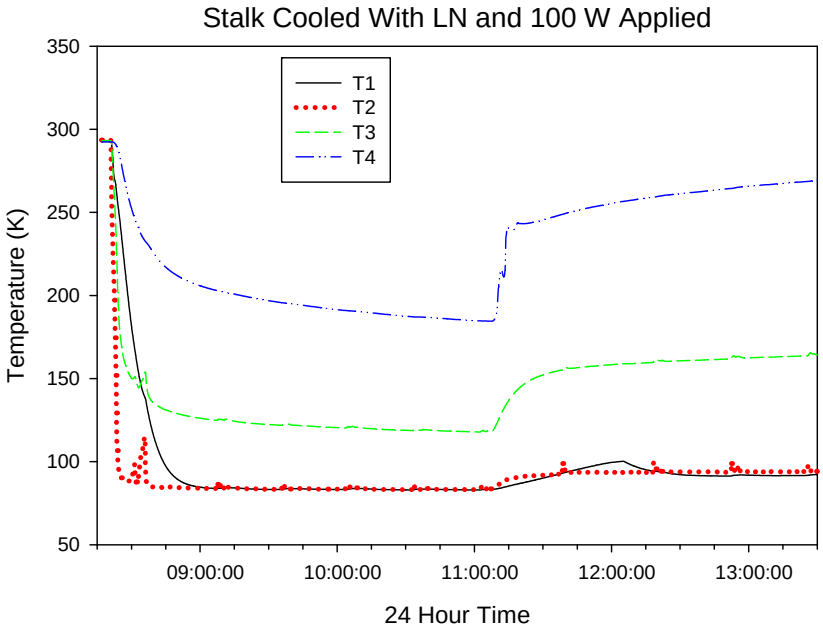


Figure 30. The stalk was cooled with LN, once the temperatures were steady. At 1107 100 W of power was applied. The spike seen at 0815 was due to pressure from the LN tank into the fill-pot being too high. The tiny bumps that can be seen along T2 are caused by the filling of the fill-pot.

The next step was to make the test stand fully automated. A new solenoid valve was received and installed so that the fill-pot levels were controlled by the liquid level controller. The regulator valve was replaced with a 10 psi pop-up relief valve to eliminate the need for capping off the regulator in-between fills. Temperature sensor diodes two and four were replaced due to an overheating casualty where temperatures were allowed to reach over 500 K due to an application of heating without any stalk

cooling. (This is analogous to operating the Mark I at full RF power with no stalk cooling, and provides a clear indication of why a stalk cooling system is required.) Later, it was discovered that the diode at T3 also received damage and would not operate in the 290 K range, but would begin working again at some random temperature, higher or lower. New diodes were ordered, but experimentation continued as the temperatures of most significance were at locations 1 and 2. The first run with the 10 psi pop-up relief valve showed interesting results. T2 still dropped very quickly while T1 took about three hours to steady out, this was also seen in subsequent tests. Once power was applied fluctuations began in T2 as can be seen in Figure 31. It seemed that the temperature rises and then decreases would both occur on a fill. This led to the hypothesis that there may be gas bubbles created where the heat was too high for the LN to remain in liquid form, and that the pressure of the fills pushed the bubbles into and or out of the cooling coil. In the positions where T2 was able to level out at minimum temperature it was measured to be ~120 K, only slightly higher than the previous configuration.

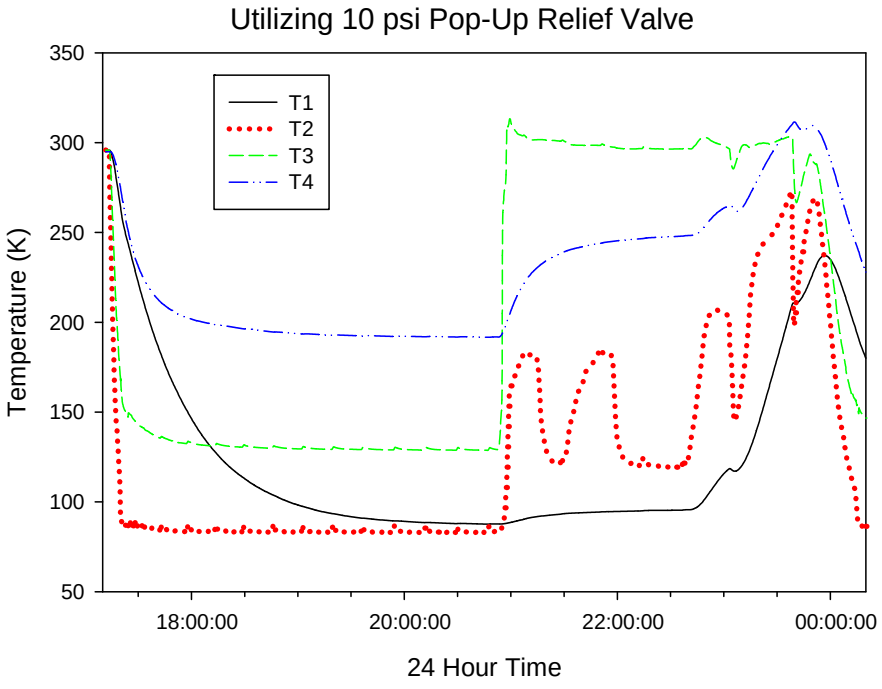


Figure 31. The system operated optimally until the power was applied at 2052. Fluctuations occurred all the way up to when the variac was turned off at 2348. No fluctuations in temperature occurred after this time.

The test was run again to see if the results were repeatable. The same fluctuations occurred after the 100 W of power was applied at 1352 as can be seen in Figure 32. Using the hypothesis that there may be gas bubbles the fill level on the fill-pot was increased from four inches to 6.5 inches at 1510 to escalate pressure on the system in hopes that it would prevent any bubbles, and eliminate the fluctuations. Initially, this seemed to work, and no fluctuations were seen for two hours; unfortunately, the fluctuations began again, but occurred less frequently. The minimum steady temperature at T2 with 100 W of power applied was again ~120 K.

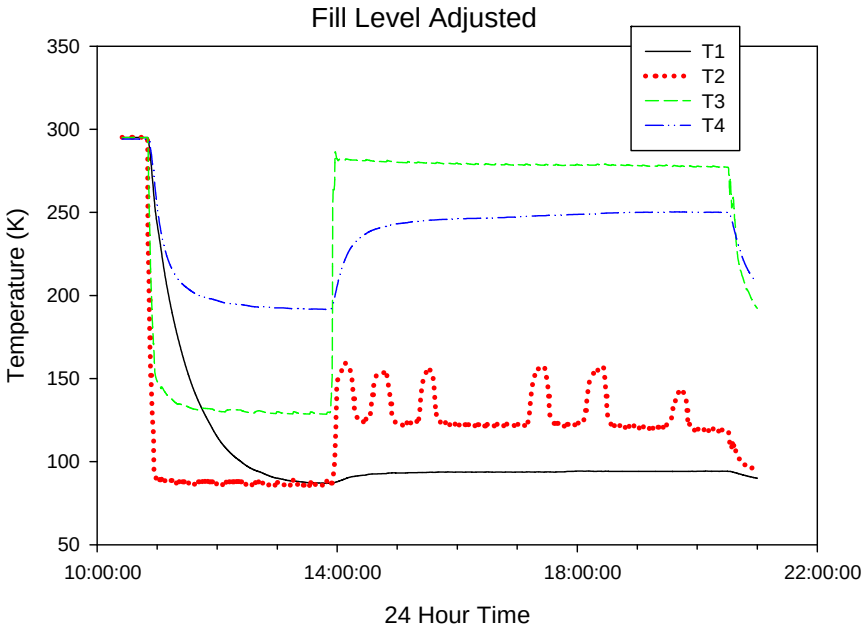


Figure 32. Cooling worked nominally until power was added. The fill level on the fill-pot was increased to create a higher pressure and flow through the system, but fluctuations still occurred.

The next step was to replace the 10 psi pop-up relief valve with a 15 psi pop-up relief valve, in hopes that the higher pressure would eliminate the temperature fluctuations. It should be noted that the pressure gauge had not been reading accurately, and it is recommended that in future testing a more accurate and reliable pressure gauge is utilized. In the first test the 15 psi pop-up relief valve worked as intended while cooling, but shortly after 100 W of power was applied at 1616 the flow out of the exhaust from the cooling coil stopped, as no gas could be felt coming out of the exhaust. This can

be seen by the temperature increases in Figure 33. The fill-pot was still maintaining liquid, and as it boiled off would refill. The LN connections to the coil were also cold so the blockage must have occurred after the LN connections but before the coil itself. At 1814 the power on the stalk was turned off, once the temperatures dropped back down to room temperature the LN began to flow through the system again, initially gas was felt coming out of the exhaust, and then liquid. The experiment was repeated to see if the results were repeatable. They were not; instead, the fluctuations from the prior experiments occurred, these are shown in Figure 34. Here, when T2 was at a steady minimum, it was measured to be ~115 K, comparable to the minimum temperatures previously measured.

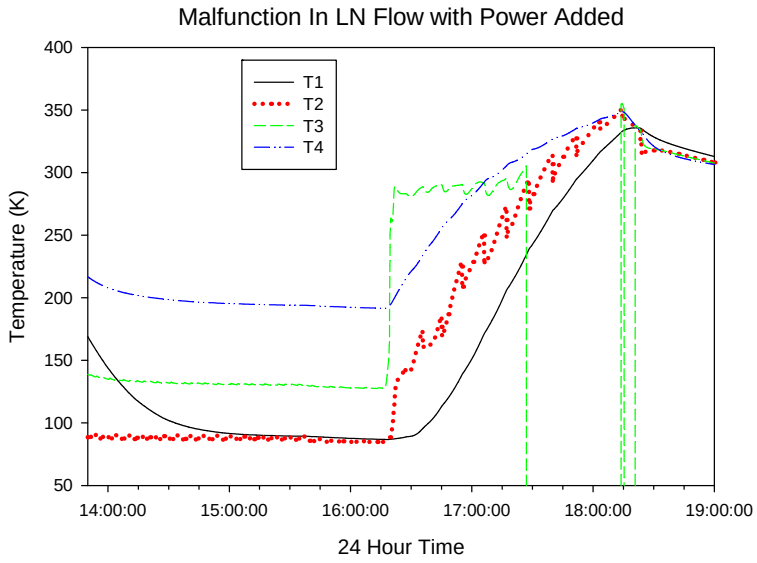


Figure 33. At 1616 the variac was turned on to 64 percent of 120 V applying 100 W of power to the stalk. Once power was applied LN flow into the cooling coil stopped. The malfunctions in the diode at T3 are apparent as dropouts in the temperature reading.

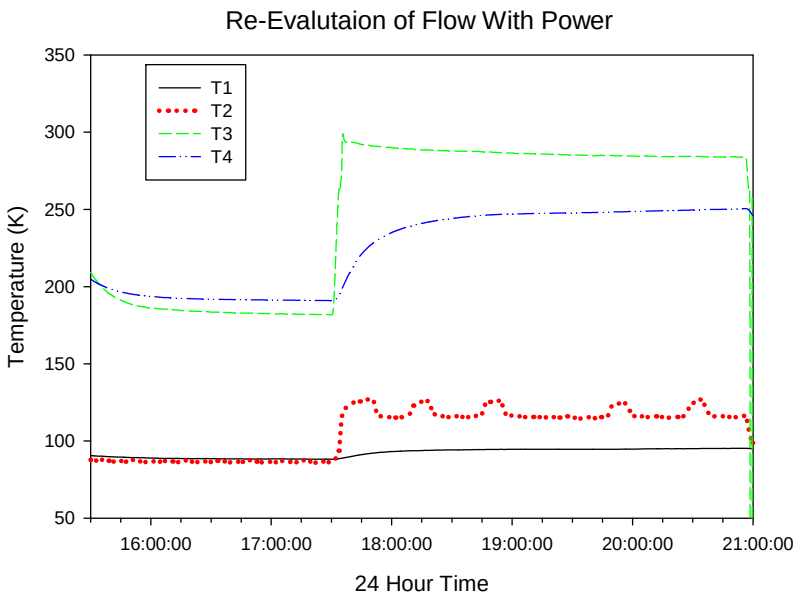


Figure 34. Instead of the LN flow stopping it continued to cool the system, but with the fluctuations seen in previous tests.

The addition of power to the automated system is the evident variable leading to the fluctuations in temperature. To determine how much power is needed to provoke the fluctuations, it was again added in increments to determine the range where the fluctuations begin. The system was cooled to equilibrium temperature, and then power was applied utilizing the variac with a 100 percent voltage of 120 V, raising it in 20 percent increments. As shown in Figure 35, the cooling system is able to steadily cool the cathode stalk with up to 37 W applied (40 percent on the variac). When the variac was increased to 60 percent (87 W) at 1806 the fluctuations immediately began, occurring almost every 25 minutes. It was observed that even though the temperature was rising in these fluctuations liquid was still coming out of the exhaust, although less than when the temperatures were on a downward trend. Currently, there is no way to measure the flow through the cooling coil or coming out of the exhaust, it is recommended this be done in future testing to help determine the cause of these fluctuations. The power range for these anomalies has been narrowed down, but the cause of them is still unknown, with gas bubbles being ruled out by the observed liquid flow that is exhausted during the temperature increases. One hypothesis is that the small diameter of tubing may be the cause of these fluctuations, testing other cooling

configurations inside of the stalk in future research will help to determine this. T2 in this test reaches its minimum at ~124 K, still within the range of the previous tests.

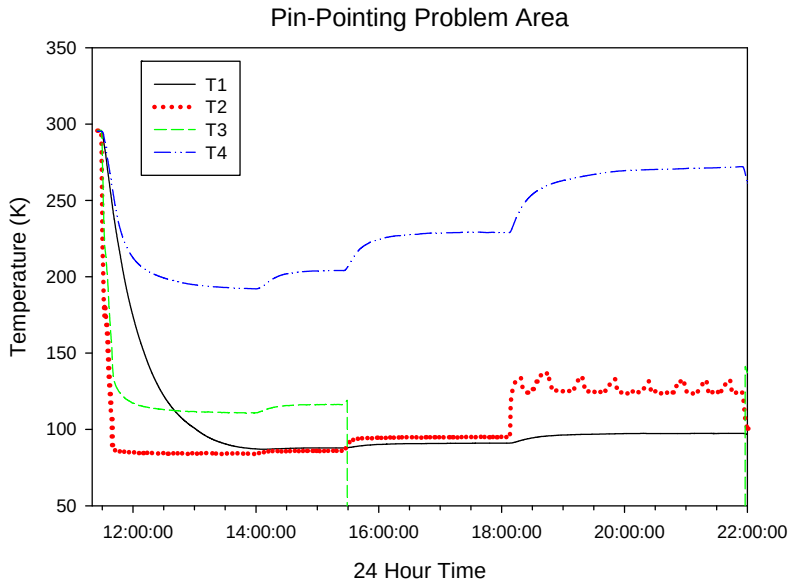


Figure 35. At 1359 the variac was turned on at 20 percent (9 W) of 120 V, then at 1525 it was increased to 40 percent (37 W). The cooling system was able to manage the power applied at these times. At 1806 the variac was increased to 60 percent (87 W). Here the fluctuations immediately began.

## C. CONCLUSIONS

Overall the test stand has been effective in replicating conditions in the MK I to allow for temperature measurements, and has shown that a cathode cooling system is a necessity for the MK I quarter-wave gun. Despite several curious results in some configurations, the overall cooling system has proven successful, with its ability to cool the cathode stalk from 439 K to ~120 K fairly consistently. Once the cause of the fluctuations is determined and corrected, the cooling system will be able to reduce a 0.93 to 3.02 W heat load increase on the helium cryostat to 0.005 to 0.017 W. This reduces the additional liquid helium needed per day from ~87 L to ~0.5 L.

To assist in determining the cause of the fluctuations, and to optimize the cooling system it is recommended that in further research a more accurate and reliable pressure gauge is installed, as well as a way to measure flow through the cooling coil. When the pressure gauge was working during manual operation, fill-pot pressure during fills

reached 15-20 psi, and in-between fills, when the regulator valve was plugged, and the LN tank valve closed, the system maintained approximately 4-5 psi. Without any differential pressure across the cooling loop, other than that provided by gravity, T1 and T2 only cooled to ~244 K, whereas with a small amount of pressure differential temperatures around 84 K could be maintained. Having a more accurate pressure gauge will allow the user to adjust for the most efficient pressure for the lowest temperatures, as well as assisting in determining the cause of the temperature fluctuations.

Another revision that could provide even more cooling is to add a cooling system to the housing for the cathode stalk. The housing itself was measured to be between 307 and 309 K when the stalk was at equilibrium temperatures with 100 W power applied and no cooling. When the stalk was at minimum temperatures with cooling only, the housing ranged from 276 K on the flange connected to the stalk (indicating that a large amount of cooling was being lost through the flange) to 297 and 298 K at HT1 and HT2. When the stalk had 100 W applied and was being cooled by the cooling coil, the housing was 305 to 307 K. It was shown that just by adding insulation during a cooling-only test that T4 could be reduced by 10K, this urges one to test the possibilities in cooling the stalk housing as well. The joint between the cathode stalk and housing must serve as a radio-frequency short as well as a mechanical support and thermal isolation, suggesting a design study trade-off between these functions would be appropriate.

Images taken by the cameras mounted at the windows viewing the tip of the cathode stalk (Figure 22) have revealed that there is no evident bending, deflection, or major changes in the cathode stalk in going from room temperature to minimum or maximum temperature. Pixel subtraction was used to determine these results in Photoshop by layering the two images and taking the difference. This is with a resolution of about 2.8 pixels per millimeter yielding a resolution displacement of ~0.35 mm displacement or ~0.34 degree deflections. The cathode stalk in the MK I gun will be supported by the Teflon "spider" besides the mounting plate making it more stable, but a more detailed and precise method for measuring these changes may be desired in future research to enable the determination of shrinkage values at cryogenic temperatures. It is

important to ensure the position of the cathode stalk does not change, and affect the transverse focusing and axial accelerating fields at the cathode tip.

It has been mentioned that cooling the cathode stalk will extend the lifespan of a cesiated photocathode. With the temperatures measured at 100 W power applied to the cathode stalk, and no cooling provided, a cesium photocathode would be inoperable on the cathode stalk. This is an additional motive for cooling the stalk, and one required for operability with this kind of cathode. This leads to the question of how the temperatures at the tip of the stalk will affect the quantum efficiency of a photocathode. Not much research has been done in this area, and the test stand can be easily modified to conduct such research. In future studies the cathode stalk test stand will be utilized for testing the effects of temperature on the quantum efficiency of photocathodes.

Lastly, it should be emphasized that the calculations for the heat load on the cryostat is an estimate only. The emissivities used in the calculation for the heat load can vary significantly based on material surface finish as well as (for some materials) the operating temperatures, and the heat load calculation is also sensitive to the exact geometry. The cathode stalk and niobium cavity are operating in very close proximity to each other, with a range of temperatures over the stalk well ranging from 4.2 K to approximately room temperature. In a worst-case scenario, the heat load caused by the stalk could be much greater, perhaps up to 20 W. If this is the case cooling the cathode stalk becomes of even more importance than it already is. It is therefore important to prepare an instrumented cathode stalk for installation into the Mark I, as the Mark I has now been cleared for high-power RF operation at NPS.

The test stand and cooling system have provided a glimpse into the inner workings of the MK I quarter-wave gun. It has shown that the temperature on the cathode stalk can vary greatly with power applied, and will have a significant effect on the cooling necessary to maintain the niobium cavity at superconducting temperatures as well as to permit the operation of high-quantum-efficiency cesiated cathodes. Liquid nitrogen has proven to be a viable source for reducing the heat load on the cryostat, as well as utilizing the helical copper tubing design to distribute the cooling to the tip of the stalk. Further research needs to be done to stabilize the operation of the cooling system,

as well as installing the temperature diagnostics on the cathode stalk inside of the MK I quarter-wave gun, based on the successful design pioneered by this thesis research. This research also provides a valuable platform for initiating research into the operation of high-efficiency cathodes in cryogenic environments, an important but heretofore unexplored area of high-power injector research.

# APPENDIX

## A. TEST STAND CATHODE STALK DIMENSIONS (cm)

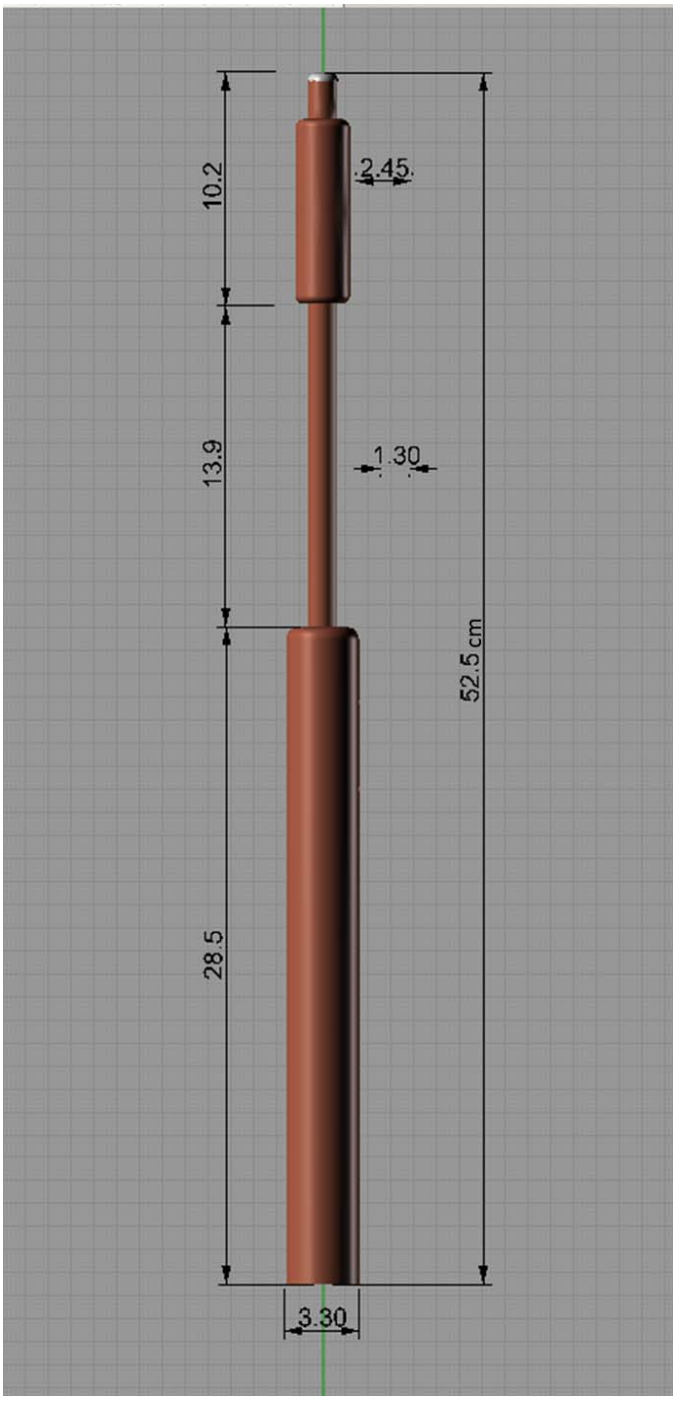

## B. VACUUM HOUSING FOR TEST STAND (cm)

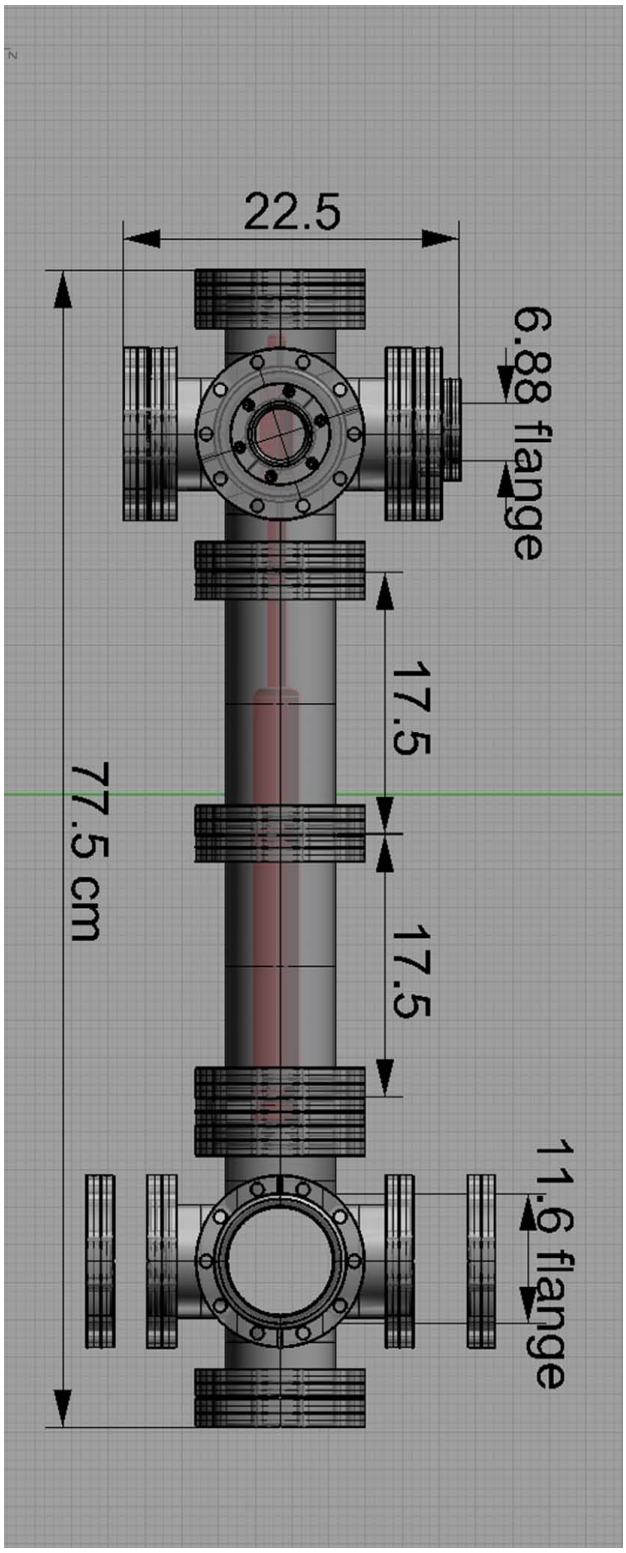

## C. INITIAL TEST STAND CONFIGURATION

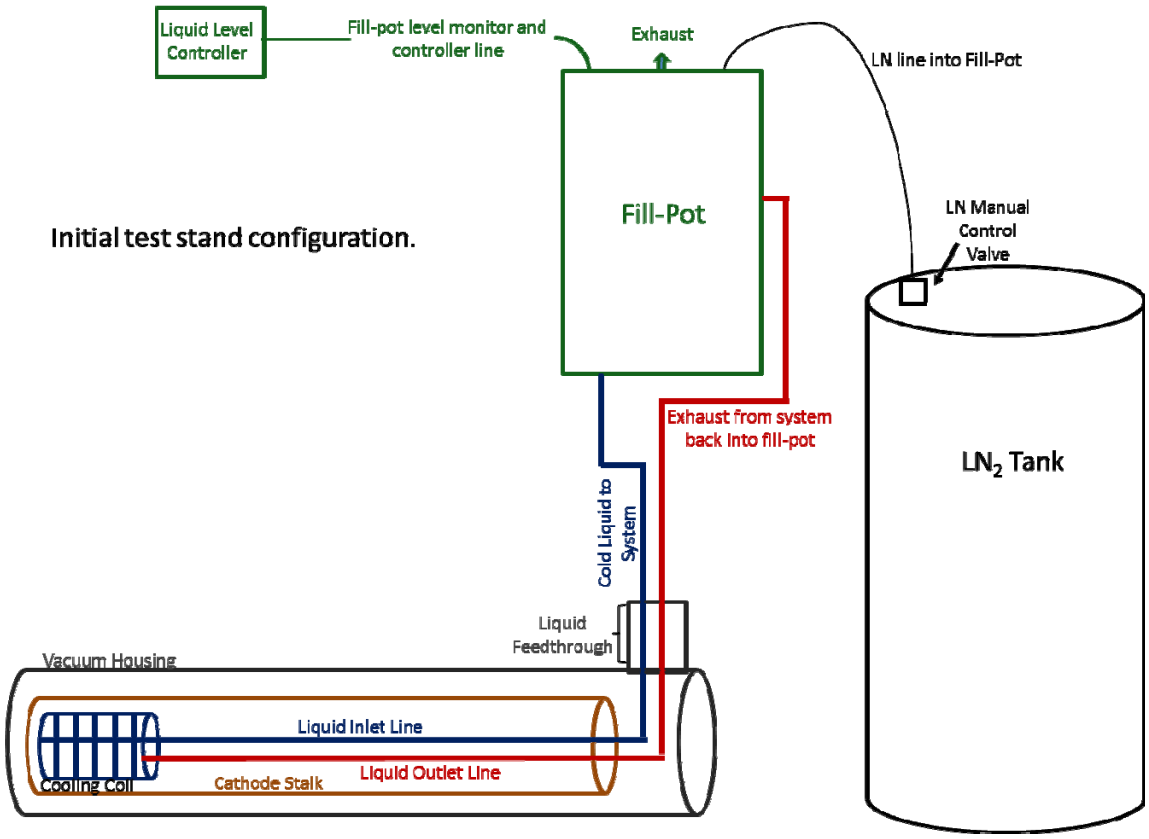

## D. CHANGE TO TEST STAND CONFIGURATION

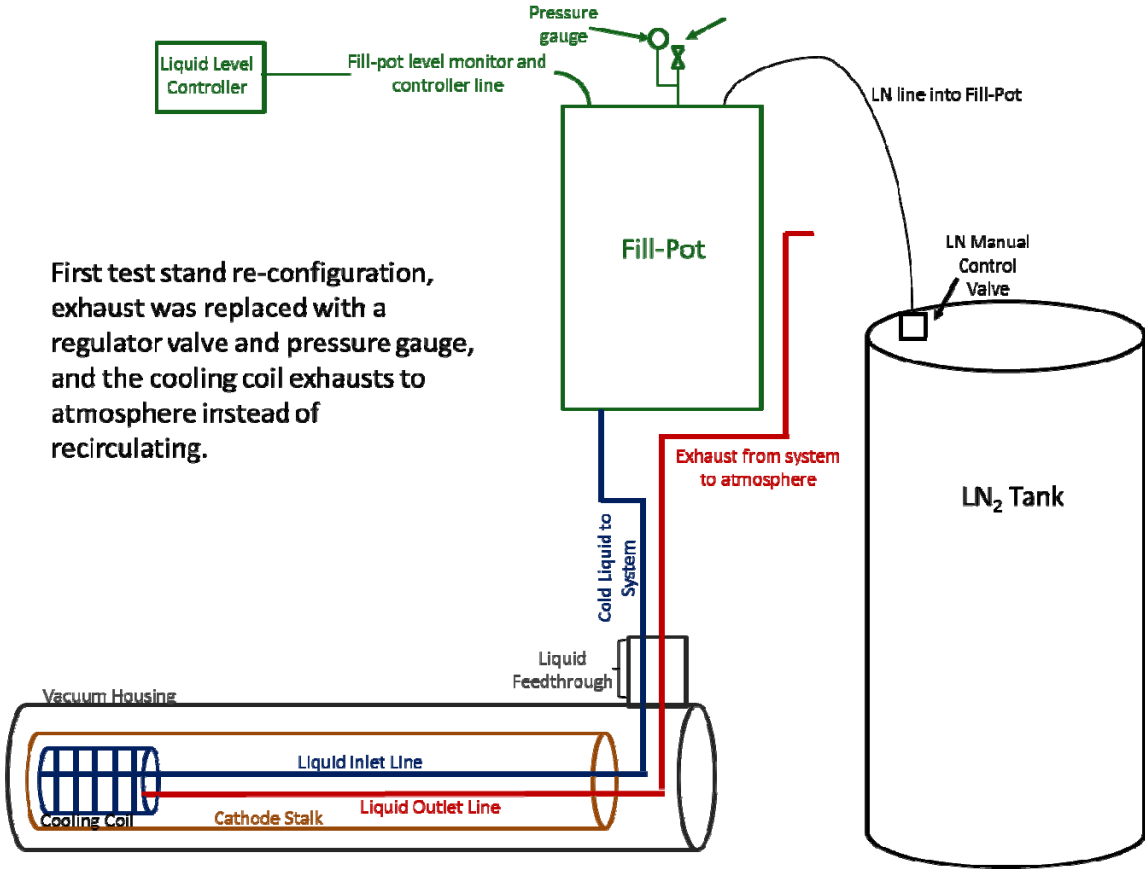

## E. FINAL CHANGE TO TEST STAND

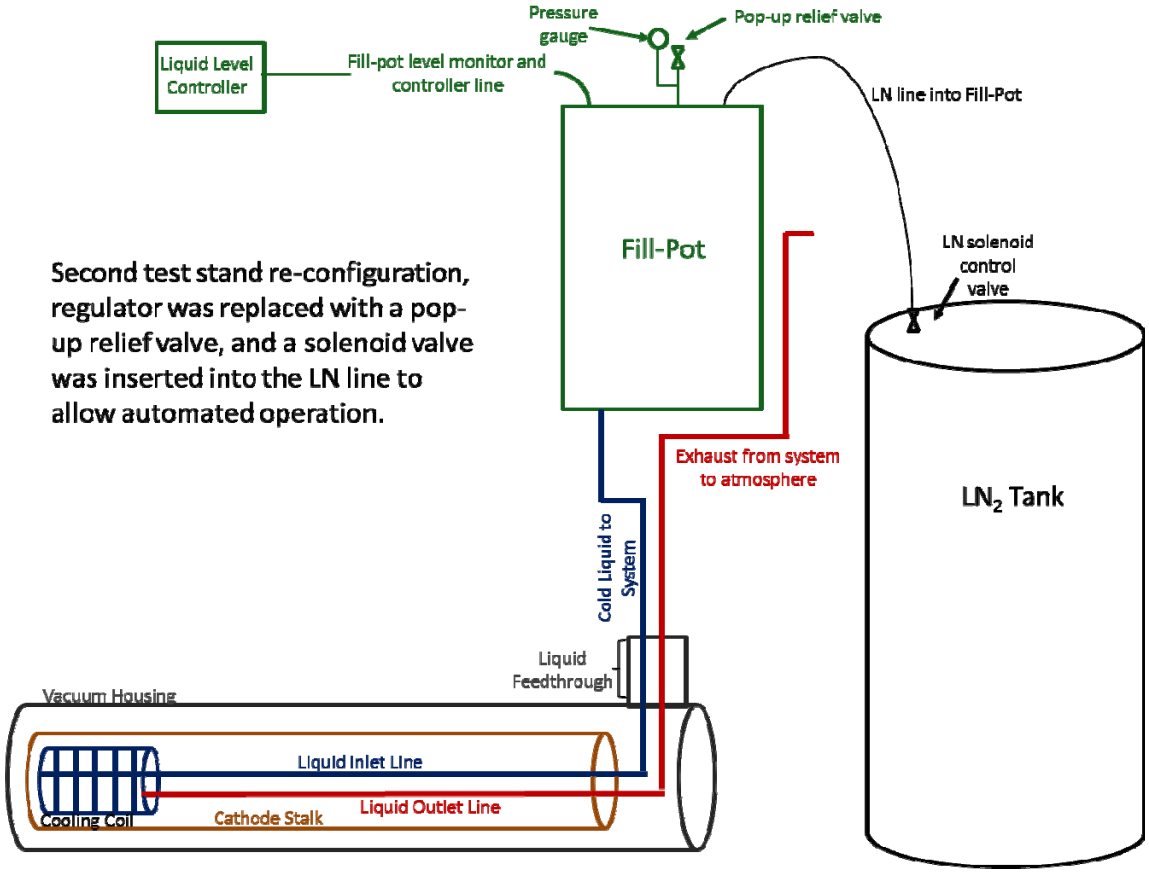

THIS PAGE INTENTIONALLY LEFT BLANK

# LIST OF REFERENCES


[1] "Laser" [Online]. Available: http://en.wikipedia.org/wiki/Laser [Accessed February 14, 2012].

[2] W. B. Colson and A. M. Sessler, "Free Electron Lasers," *Annual Review of Nuclear and Particle Science*, vol. 35, pp. 25–54, December 1985.

[3] T. C. Katsouleas et al., *Scientific Assessment of High-Power Free-Electron Laser Technology*. Washington, D.C., The National Academies Press, 2009, pp. 14–38.

[4] W. B. Colson, "Free Electron Lasers," class notes for PH4858, Department of Physics, Naval Postgraduate School, Fall 2012.

[5] J. Rathke et al., "Design and fabrication of an FEL injector cryomodule," in *Proceedings of 2005 Particle Accelerator Conference Proceedings*, Knoxville, TN, pp. 3724–3726, 2005.

[6] Centre Laser Infrarouge d'Orsay, "What is a Free Electron Laser?" [Online]. Available: http://clio.lcp.u-psud.fr/clio eng/FELrad.html [Accessed March 8, 2012].

[7] W. B. Colson, "Free Electron Laser physics," class notes for PH4055, Department of Physics, Naval Postgraduate School, Summer 2011.

[8] W. B. Colson, C. Pellegrini, A. Renieri, "Classical Free Electron Laser Theory," in *Free Electron Laser Handbook*, vol. 6, ch. 5. North-Holland Physics, 1990.

[9] J. R. Harris et al., "Design and operation of a superconducting quarter-wave electron gun," *Physical Review Special Topics—Accelerators and Beams*, vol. 14, issue 5, article 053501. American Physical Society, 2011. http://prst-ab.aps.org/pdf/PRSTAB/v14/i5/e053501

[10] A. Arnold and J. Teichert, "Overview of superconducting photo injectors," *Proceedings of the 2009 Superconducting RF Conference*, Berlin, Germany, Rep. MOOBAU03, 2009.

[11] S. P. Niles et al., "NPS prototype superconducting 500 MHz quarter-wave gun update," *Proceedings of the 2010 FEL Conference*, Malmo, Sweden, Rep. WEPB28, 2010.

[12] Z. S. Spakovszky, "Thermodynamics and propulsion: Radiation heat transfer between planar surfaces." Internet: http://web.mit.edu/16.unified/www/SPRING/propulsion/notes/node134.html, Feb. 1, 2002 [Accessed May 16, 2012].

[13] D. Shaw, B. N. Watts. “Evaporated films of niobium,” *British Journal of Applied Physics*, vol. 11, pp. 304–305, Jul. 1960.

[14] “Table of total emissivity” [Online]. http://www.monarchserver.com/TableofEmissivity.pdf [Accessed May 16, 2012].

# INITIAL DISTRIBUTION LIST

1. Defense Technical Information Center
   Ft. Belvoir, Virginia

2. Dudley Knox Library
   Naval Postgraduate School
   Monterey, California

3. Prof. John W. Lewellen
   Naval Postgraduate School
   Monterey, California